Scale-up of Solvent Injection Processes in Post-CHOPS Applications

by

Juan Jose Martinez Gamboa

A thesis submitted in partial fulfillment of the requirements for the degree of

Master of Science

in

Petroleum Engineering

Department of Civil and Environmental Engineering

University of Alberta

Abstract

Cold Heavy Oil Production with Sand (CHOPS) is widely used as a primary non-thermal production technique in thin heavy oil reservoirs in Western Canada and some other regions in South America. It has been reported that more than 85% of the original oil in place remains trapped in-situ, requiring additional follow-up (i.e., post-CHOPS) recovery strategies to be implemented. Solvent-aided processes, such as cyclic solvent injection (CSI), are commonly adopted due to the particular thin pay zone, which renders the application of thermal approaches uneconomical. It is widely accepted that configuration of wormhole networks (i.e., high-permeability channels caused by sand production) and foamy oil flow are key characteristics pertinent to these processes, and they play an important role in the overall success. Field-scale flow simulations are often performed to approximate the reservoir response and to optimize operating strategies. However, grid block sizes in field-scale models are generally much larger than the wormhole scale, and numerical analysis is often performed by arbitrary adjustment of dispersivity. This thesis proposes a practical workflow to scale up these mechanisms for field-scale simulations in wormhole networks that span over multiple scales.

First, a set of detailed high-resolution (fine-scale) simulation models, where both matrix and high-permeability wormholes (modeled as fractal networks) are represented explicitly in the computational domain, is constructed to model how the solvent propagates away from the wormholes and into the bypassed matrix. Next, a dual-permeability approach is adopted to facilitate the scale-up analysis. Solvent transport and additional mixing in wormhole networks

can be captured by parameters such as shape factor and effective dispersivity in an equivalent coarse-scale dual-permeability system. Bivariate distributions of effective longitudinal/transverse dispersivities and wormhole intensity are constructed and calibrated by minimizing the difference in recovery response (i.e., profiles of gas/oil production) between the detailed model and an equivalent dual-permeability continuum model.

Finally, field-scale simulations are constructed using average petrophysical properties and initial conditions (fluid saturations, pressure distribution, and wormhole development) commonly encountered at the end of CHOPS. Multiple field injection scenarios (i.e., of different number of cycles and durations of the soaking period) are simulated and analyzed. As expected, extended soaking period is more beneficial in terms of ultimate oil recovery (slower decline in oil rate), but it also reduces the early production rate. These observations can be attributed to the fact that a longer soaking period may prolong the production phase by increasing the effective drainage area contacted by the solvent; however, the amount of solvent in the near well region is also diluted. Interestingly, when an economic limit (i.e., minimum oil producing rate) is imposed, the optimal soaking time is not necessarily the longest one. It depends on the trade-off between extracting additional oil recovery at late times versus producing at a higher rate at early times. The analysis also reveals that during the implementation of multiple consecutive cycles, the two initial cycles contribute the most to the final oil recovery. Therefore, injecting larger volumes of solvent and extending the soaking times are recommended strategies during the first and/or second cycles. In addition, when the amount of solvent available is limited, the results support in the strategy of injecting all the solvent in one single consolidated cycle, with an extended soaking period, rather than performing shorter consecutive cycles.

Dedication

This work is proudly dedicated to both my GrandFathers: Juan Francisco and Angel Elias, who have eternally been present in ways no one could ever imagine. They have always reinforced the importance of love, dedication, and persistence in every aspect of this journey.
Without their support, this dreamed adventure would not have become a reality.

I would also like to dedicate these efforts to my beloved family, their constant support and guidance have always empowered me to chase my dreams and be where I am today.

Acknowledgements

First and foremost, I would like to express my gratitude and deepest appreciation to my Supervisor, Dr. Juliana Leung, who has been the leader and greatest supporter of this work. I thank her for relying on me from the very first day and for always providing her bright ideas and continuous support during my graduate studies. Her attitude and empowering abilities were the keys to the successful development of this project. I will forever be grateful to her for giving me the opportunity to work with her Research Group, and I look forward to continuing receiving her valuable advice during my professional journey.

I also want to express my special gratitude to Dr. Huazhou (Andy) Li and Dr. Zhehui (Charlie) Jin for being part of my examination committee. Their comments and recommendations were always appreciated.

Thanks to my research buddies and personal friends who have supported me in every possible way over the course of my graduate studies. Their sole presence has made these two years a very enjoyable experience. They have enriched my life in many ways and will surely become life-long friends. I would like to think that our life paths will hopefully cross again at some point in the future.

Finally, my gratitude goes to the Petroleum Technology Research Centre (PTRC) for providing the financial support for this research work under the Heavy Oil Research Network (HORNET) Program, and to the Computer Modelling Group Ltd. (CMG) for providing academic licenses of their reservoir simulation suite (IMEX, GEM, STARTS, WinProp, and CMOST).

Table of Contents

List of Tables

List of Figures

Nomenclature

Symbols

T	=	Thickness (m)
T_{HALF}	=	½ of entire model Thickness (m)
N	=	Total number of layers
$\emptyset_{F(DK)}$	=	Fracture porosity in the equivalent coarse-scale Dual-Perm model
$\emptyset_{M(DK)}$	=	Matrix porosity in the equivalent coarse-scale Dual-Perm model
V	=	Volume
$\emptyset$	=	Porosity
V_{coarse}	=	Coarse block bulk volume (Dual-Perm)
L	=	Fracture spacing (m)

Subscripts

i	=	Layer index
WH	=	Wormhole
M	=	Matrix
x, y, z	=	Coordinates

Greek Letters

α_L	=	Longitudinal Dispersivity
α_T	=	Transverse Dispersivity
σ	=	Shape Factor

Acronyms

CHOPS	=	Cold Heavy Oil Production with Sand
CSI	=	Cyclic Solvent Injection
DLA	=	Diffusion-Limited Aggregation
EOR	=	Enhanced Oil Recovery
HM	=	History Match
HOB	=	Heavy Oil Belt
OOIP	=	Original Oil in Place
SAGD	=	Steam-Assisted Gravity Drainage
UCSS	=	Unconsolidated Sandstone
VAPEX	=	Vapor Extraction
WCSB	=	Western Canadian Sedimentary Basin
WI	=	Wormhole Intensity

Chapter 1: Introduction

1.1 Background and Motivation

Cold Heavy Oil Production with Sand (CHOPS) is a common reservoir development approach to produce heavy oil resources from thin and unconsolidated sandstone reservoirs in Western Canada and Venezuela. This approach works well during primary production before the reservoir pressure is too depleted or wells water out. At this point, when the economic limit has been reached, most of these reservoirs exhibit a very low recovery factor in the range of 5 to 15% of the OOIP.

Predicted shortfalls in conventional resources and the large volumes of heavy oil reserves, not only in Western Canada and Venezuela but also in other parts around the globe make these resources very attractive to investors. The potential and promise of these heavy oil resources depend on the successful development and implementation of follow-up enhanced oil recovery practices that permit the extraction of even more recoverable volumes. Cyclic solvent injection (CSI) has been widely accepted as the best enhanced oil recovery (EOR) approach for these reservoirs and has even been subjected to pilot testing in recent years.

The development of complex high-permeability channels (i.e., wormholes) in the subsurface formations introduces new challenges that have not yet been fully covered by commercial simulators. Additional sub routines that account for the wide range of wormhole networks with their complex configurations and capture the actual physics are essential for improving the validity of numerical simulations. To efficiently redevelop these CHOPS heavy oil reservoirs, it is essential to have reliable modeling approaches that provide a better

understanding of the impact of parameters such as solvent type and injection schemes in the ultimate oil recovery.

Although multiple modeling approaches have been proposed in the literature before, there is not a consensus as to which one better represents the true recovery response. The use of different modeling approaches leads to different recovery results, therefore increasing the uncertainty surrounding the actual outcome.

Significant improvements to the design and implementation of post-CHOPS enhanced oil recovery (EOR) methods, such as cyclic solvent injection (CSI) can be achieved by developing a reliable numerical simulation framework that permits a better understanding of the interactions between the solvent and heavy oil in wormhole networks that span over multiple scales.

1.2 Problem Description

The success of cyclic solvent injection (CSI) processes often depends on the ability of the solvent to contact the oil. Numerical simulations are needed for analysis of pilot or field-scale applications. The ability to extrapolate lab-scale measurements to the simulation modeling scale is extremely important since these processes require the solvent to get from the wormhole into the oil, and diluted oil to drain faster than solvent can evolve with dropping pressure. However, since the modeling scale is typically much larger than the wormhole's size, incorporating lab-scale diffusion data (which often neglects the effects of wormholes) is not trivial. In the end, it is necessary to quantify the effects of heterogeneities below the modeling resolution for realistic predictions using these numerical models.

Common field-scale simulations are performed with a minimum grid block size of 1 to 5 m, which is well above the wormhole scale. Therefore, not fully incorporating the varying wormhole characteristics in field-scale applications can lead to erroneous and misleading results. Although previous numerical studies have examined the optimization of cyclic solvent injection (CSI) processes, a lack of proper scale-up procedures has rendered their description of heterogeneous wormhole networks at the field scale incomplete. The common weakness of some preceding modeling approaches is that they do not describe the varying wormhole characteristics in field-scale applications, failing to provide a better representation of the solvent and heavy oil interactions in the reservoir.

This misrepresentation could potentially compromise the reliability of the corresponding optimization results. It is argued that the model employed in this study could better represent the detailed wormhole features at the coarse scale; hence, it is more appropriate for field-scale operations design.

1.3 Research Objectives

The main theme of this research is to improve the modeling of post-CHOPS applications, in which complex wormhole networks play a significant role in solvent transport mechanisms, by introducing a scale-up workflow that accounts for the spatial variations in wormhole characteristics. To address this overarching theme, as series of specific objectives have been identified:

(1) Construct a series of high-resolution fine-scale models with complex wormhole networks modeled as fractals in order to explicitly simulate solvent transport mechanisms in the computational domain.

(2) Propose a scale-up methodology that allows the construction of models at a coarser scale (with less number of grid blocks) by assigning representative properties (fracture and matrix porosity, shape factor, and effective dispersivity) to a dual-permeability continuum in such a way that they properly capture the subscale heterogeneities. Hence, minimizing the difference in oil and gas recovery between the detailed model and an equivalent dual-permeability continuum model.

(3) Use a series of calibration models to construct bivariate distributions of effective dispersivity and wormhole intensity. These distributions can be fitted to conditional Gaussian distributions that can later be sampled in a statistical approach when constructing equivalent (or effective) coarse-scale models.

(4) Validate the robustness of the proposed workflow by contrasting the recovery response (i.e., profiles of gas/oil production) from a large fine-scale model and its equivalent coarse-scale dual-permeability continuum.

(5) Using the scale-up approach, evaluate certain operational parameters, such as solvent injection rate, soaking time, and number of cycles, by performing sensitivity analyses to provide

insights on operational strategies and key considerations when optimizing cyclic solvent injection (CSI) processes in field-scale applications.

1.4 Thesis Outline

Chapter 1 covers the main aspects of this research work by briefly presenting the background and motivation, introducing the problem description, and explaining the specific objectives that have to be met in order to achieve the ultimate purpose of this work.

Chapter 2 presents a comprehensive review of Cold Heavy Oil Production with Sand (CHOPS), starting with the historical development of this technology and describing the main production mechanisms associated with this practice. The review then continues to describe the state-of-the-art in post-CHOPS follow-up applications and their current limitations. A critical discussion of the strengths and weaknesses of various modeling approaches that have been presented in the literature in recent years follows in an attempt to illustrate the gaps and the challenges that are to be addressed in this study.

Chapter 3 describes each one of the steps that were followed in the development of this framework to scale up solvent transport mechanisms in wormhole networks. This chapter covers the construction of the static reservoir simulation model as well as the dynamic section (injection, soaking, and production schemes). It illustrates how to migrate from a fine-scale to a coarse-scale dual-permeability without ignoring relevant subscale heterogeneities.

Chapter 4 illustrates the application of the scale-up workflow in a large scale application. The coarse-scale model is validated against the corresponding fine-scale high-resolution model in order to test the validity of the scaled-up values used in the dual-permeability continuum.

Chapter 5 is focused on the construction of a series of field-scale models to optimize the design of post-CHOPS applications in the field. Parameters such as soaking time, number of cycles, and amount of solvent are examined in order to propose an optimal recovery strategy.

Chapter 6 finally presents the conclusions and main contributions of this work as well as some recommendations for future developments in the subject.

1.5 Novelties and Contributions

This work presents a novel practical workflow to scale up solvent transport mechanisms from a high-resolution fine-scale to a coarse-scale. This approach is used to properly assign relevant parameters to an equivalent dual-permeability model (e.g., dispersivities, shape factors) in accordance with the grid size and wormhole intensity at the fine scale. This framework takes into account the impacts of sub-scale heterogeneities (i.e., wormhole properties and spatial configuration at the fine-scale). The results have facilitated the formulation of a systematic workflow for representing multiple wormhole networks in field-scale dual-permeability models.

Significant improvements to the design and implementation of these enhanced oil recovery (EOR) methods can be achieved by the development of reliable numerical simulation

approaches that allow a better understanding of the solvent and heavy oil interactions in wormhole networks that span over multiple scales. The outcomes would help considerably in the design of production/development strategies and assessment of solvent transport in post-CHOPS recovery processes. In this thesis, field-scale simulations are performed to examine various aspects pertinent to the operation of CSI processes, while several recommendations are concluded from the results.

Chapter 2: Literature Review

2.1 Cold Heavy Oil Production with Sand (CHOPS)

2.1.1 Historical Development

Primary recovery in conventional hydrocarbon resources relies completely on natural forces within the reservoir (i.e., solution gas, gas cap, and fluid or formation expansion). These in-situ drive mechanisms work successfully for light oils, which typically have a low viscosity and high mobility at reservoir conditions (i.e., pressure and temperature). Nevertheless, when it comes to heavy oil extraction, these natural forces might not be as effective as they are in conventional plays due to the fact that heavy oils are not always sufficiently fluid at downhole conditions.

Artificial lift methods are then required to aid in the vertical lift of heavy fluids from the reservoir to the surface. Conventional artificial lift devices, such as beam pumps, gas lift valves, and electrical submersible pumps (ESP) are not very efficient in handling heavy fluids that carry high amounts of solids (sandy particles from unconsolidated layers). This limitation explains why the first discoveries of heavy oil in Canada and Venezuela did not seem very promising in terms of commercial exploitation.

The development of progressing cavity pumps (PCP) in the 80's, as artificial lift devices capable of handling large amounts of sand from shallow reservoirs, brought attention to the thin and unconsolidated heavy oil deposits in the Western Canadian Sedimentary Basin (WCSB). The first discoveries had been made in Eastern Alberta and Western Saskatchewan, around the Lloydminster area in the late 20's.

Most of the heavy oil unconsolidated sandstone (UCSS) deposits in Alberta are found in the Lower and Middle Mannville Group, which is an undeformed and flat-flying Middle Cretaceous clastic sequence comprised of sands, silts, shales, a few coal seams, and some thin concretionary beds (Dusseault, 2002). The Bakken Formation, mainly found in Saskatchewan, also exhibit similar petrophysical characteristics (thickness and average porosity and permeability).

Operators observed that wells without any downhole equipment for sand control had a tendency to initially produce more oil than those with complex sand exclusion devices. However, excessive sand production and high oil viscosity (low flow rate) rendered most wells uneconomical. The surge in oil prices in the early 80's encouraged adapting new completion strategies to promote oil and sand production: sand control devices were no longer installed downhole and wellbore perforations were designed to be of a larger diameter. Canadian experiences and practices were soon replicated in Venezuela, where heavy oil deposits located in the Orinoco heavy oil belt are of similar characteristics. Fig. 2.1 shows the location of the main CHOPS assets in Canada and Venezuela. Table 2.1 compares the typical reservoir properties of UCSS heavy oil deposits in Saskatchewan and the Orinoco heavy oil belt.

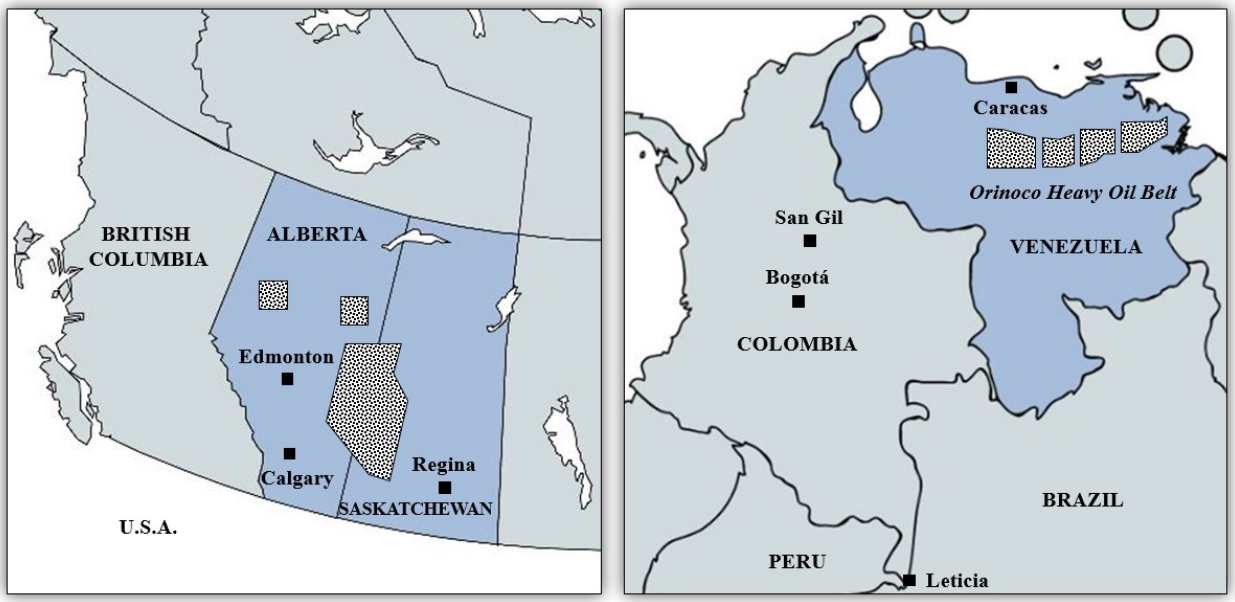

Fig. 2.1 – Location of CHOPS assets in Western Canada and Venezuela

Table 2.1 – Comparison of typical average reservoir properties in Canada and Venezuela

[Adapted from Dusseault (2002)]

Parameter	Units	Alberta and Saskatchewan Canada	Orinoco Heavy Oil Belt Venezuela
Depth	m	730-850	450-650
Thickness	m	3-15	20-80
Initial Reservoir Pressure	MPa	6-7	4.5-6.5
Reservoir Temperature	Celsius	30	60
Average Porosity	Fraction	0.30	0.31
Permeability	Darcy	2-4	5-15
API		11-13.5	8-10
Viscosity (Dead Oil)	cP	1,400	1,000

2.1.2 Production Profile

Provided that the heavy oil resources can be initially extracted without any additional energy (i.e., steam or solvent injection), operators will try to produce as much heavy oil as possible by primary recovery methods (Speight, 2009). The production from these reservoirs is initially driven by solution gas, sand production, and foamy oil, which have been identified as the main production mechanisms in these particular heavy oil deposits.

Although most of these heavy oil reservoirs in Western Canada usually have downhole temperatures in the range of 20 to 30 degrees Celsius, which is significantly lower than that in other conventional deposits, the term "cold production" has also been used in other countries like Venezuela, where temperatures are much higher. Therefore, the term "cold production" refers to primary recovery without any thermal application and it is not necessarily limited to low reservoir temperatures.

This cold production strategy is characterized by a large initial sand influx, which accounts for 30-40% of the produced slurry volume (gas-free liquids and solids). After reaching a maximum sand cut after the initial few months, sand production gradually decreases to less than 10% of the total volume of slurry (Dusseault, 2002; 2007) and tends to stabilize at low cuts that are usually in the range of 0.1 to 5% (Maini, 2001). It is often observed that sand cut is directly correlated with the oil viscosity (i.e., more viscous oils tend to carry more sand). The multicomponent slurry (oil/gas/water/sand) goes to stock tanks in which gravity segregation is the main separation mechanism.

Oil rate tends to increase gradually over a period of several months to a peak value of 20-40 m^3/day, and after which, it gradually decreases to uneconomical in the range of 2-3 m^3/day (Dusseault, 2002).

Reservoir pressure also shows a slower decline and gas-oil ratio (GOR) remains low (typically less than 15 sm^3/m^3) under this production mechanism.

Fig. 2.2 shows the typical production trend of a well producing under CHOPS. This particular trend is known as "CHOPS signature", due to the fact that the majority of wells follow this behavior. Note that three production cycles, separated by workovers, can be identified as attempts to promote more sand influx and to boost oil production. Production rate generally drops dramatically once the sand production stabilizes at a low rate, rendering a relatively low recovery factor (<10%) in most of the cases. Therefore, these wells are excellent candidates for potential enhanced oil recovery (EOR) follow-up applications, which have been subject to extensive studies and pilot testing over the last few years.

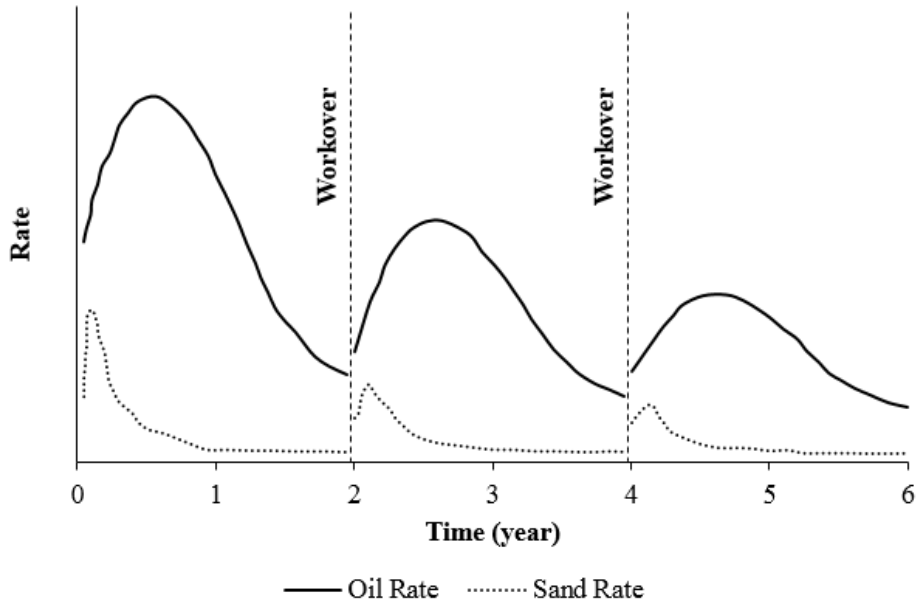

Fig. 2.2 – Typical CHOPS signature

2.1.3 Sand Production and Wormhole Development

Operators in Western Canada observed that vertical wells operated at high drawdown pressures and without downhole sand exclusion devices performed better than those with sand control devices (i.e., slotted liners or sand screens). Oil rates were reported to be as much as 10 times higher compared to their sand-controlled counterparts (Maini, 2001). These field observations led to the redesign of well completion strategies to promote the production of sand as opposed to the conventional approaches.

Sand production, which contributes to the development of high-permeability channels, commonly known in the industry as wormholes, is undoubtedly one of the main production mechanisms in CHOPS alongside with foamy oil.

Early field observations proved that wells located even further than a few hundreds of meters apart were interconnected by wormhole networks (Yeung, 1995), as evidenced by tracer surveys and experiments with fluorescein dyes. In addition to this, in-fill wells commonly experience fluid losses during drilling, which has been attributed to the wormhole networks created by previously-drilled nearby wells.

Sand failure and fluidization are controlled by a geomechanical constraint; a particular wormhole would grow if the pressure gradient exceeds certain critical threshold; the network tends to expand in areas of lower cohesive strength (Sharifi Haddad and Gates, 2015). Experiments conducted in sandpacks by InnoTech Alberta (formerly known as Alberta Research Council) revealed that the wormhole diameter would vary along the network, ranging between 2.5 cm to 30 cm (Tremblay et al., 1998; Liu and Zhao, 2005); it typically increases from the perforations at the wellbore along up to a maximum value and then continuously decreases towards the tip. Wells that have typically produced at average rates of 10 to 20 m^3/day can finish

their lifespan with large volumes of cumulative sand in the range of 500 to 1,000 m^3 (Maini, 2001).

2.1.4 Foamy Oil Flow

The other recovery mechanism, which is closely associated to solution-gas drive is a non-Darcy type of two-phase flow, commonly known as "foamy oil". This term evolved from field observations when operators noticed that the produced oil was in the form of thick oil-continuous stable foams (Maini, 2001). Liquid samples collected at the wellhead would eventually shrink provided that they remained undisturbed for some time. The so-called foamy oil is a non-equilibrium phenomenon where gas bubbles are dispersed in a continuous oil phase seeming reluctant to coalesce and form a continuous gas phase.

In conventional fluids, once the pressure falls below the thermodynamic bubble point, dissolved gas starts to evolve in the form of small bubbles that grow and tend to coalesce to form a continuous gas phase known as free gas. Once this continuous gas phase reaches certain saturation, it starts to flow resulting in an increase in the gas-oil ratio (GOR). In contrast, foamy oil causes reservoir pressure to decline slower and producing gas-oil ratios (GOR) remain low.

Fig. 2.3 illustrates the development of foamy oil starting from dissolved gas Fig. 2.3 (a), continuing to bubble nucleation when the reservoir pressure drops below the bubble point Fig. 2.3 (b), and the later formation of a continuous gas phase that flows to the wellbore Fig. 2.3 (c).

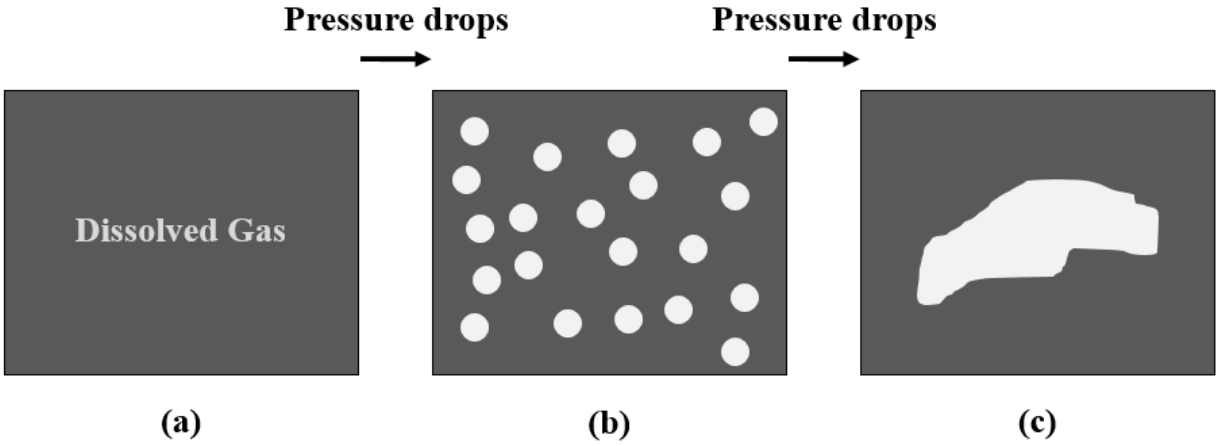

Fig. 2.3 – Schematic of foamy oil flow

(a) Dissolved gas; (b) Bubble nucleation; (c) Formation of a continuous gas phase

As a result of this phenomenon, primary recovery factors are usually higher than expected and well productivities are higher than the rates calculated by conventional inflow equations. This anomalous production behavior has been subject to multiple studies which have tried to find alternative ways to describe and capture the on-going physics of this phenomenon for reservoir simulations and inflow predictions.

Common approaches for modeling foamy oil can be divided into two broad groups: equilibrium models and kinetic approaches (Maini, 2001). Fig. 2.4 illustrates the subdivisions of the most commonly-used foamy oil numerical formulations.

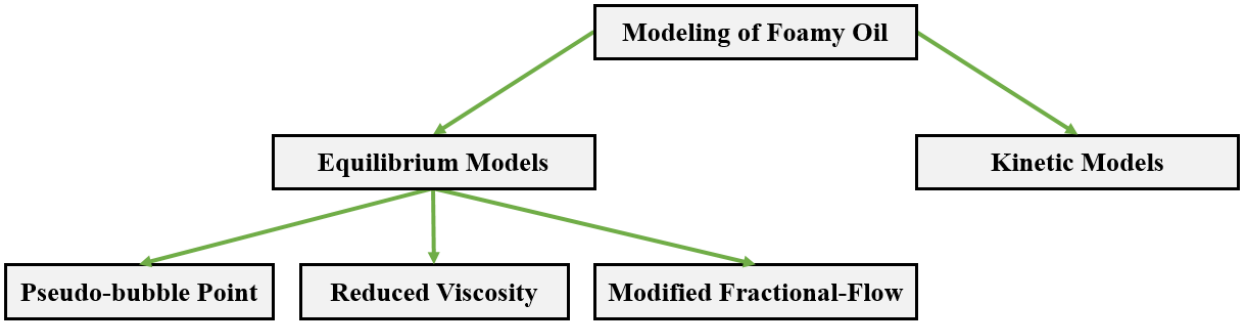

Fig. 2.4 – Commonly-used approaches to model foamy oil

Equilibrium models are known this way due to the fact that most commercial reservoir simulators assume that all phases (liquid/gas) at reservoir conditions are at complete local thermodynamic equilibrium. They are fairly easy to implement, which explains why they have attracted considerable attention in recent studies. These models, however, are unable to capture the thermodynamic stability of foamy oil dispersions at different operating conditions. Therefore, it remains challenging to predict the impact of varying operating conditions for different fluids. Equilibrium models include the pseudo-bubble point, reduced viscosity, and fractional flow models.

The pseudo-bubble point model was first introduced by Kraus et al. (1993) and has been successfully implemented in multiple compositional reservoir simulators (CMG-GEM, 2016). This approach uses the bubble point pressure as an adjustable parameter. This formulation claims that there seems to be certain pressure (below the true thermodynamic bubble point) at which the gas bubbles entrained in the foam coalesce to become a continuous free gas phase. This model requires the manipulation of the equilibrium ratios (k-values) to model this behavior. The outcome of this approach is successful in representing the three main field observations in foamy oil reservoirs: natural pressure maintenance, low gas-oil ratio (GOR), and high oil recovery.

The reduced viscosity model, unlike other equilibrium approaches, accounts for an apparent adsorption of asphaltenes by the surface of the tiny bubbles that are constantly evolving. Claridge and Prats (1995) claimed that this "asphaltene coating" stabilizes the bubbles at a small size. This apparent removal of dispersed asphaltenes from the liquid phase and its transfer to the bubbles could explain the reduction in viscosity when foamy oil is the driving mechanism. This approach, however, have not been fully verified by means of laboratory testing (Maini, 2001).

The modified fractional-flow model is arguably a very common approach in reservoir simulation studies. This approach attempts to represent the actual production behavior (oil recovery response) by modifying the gas/oil relative permeability functions. It is assumed that the solution gas that evolves as pressure falls below the bubble point remains entrained in the oil phase to up to a certain limiting entrained gas saturation. Any further gas liberation, beyond this point (limiting saturation) results in a continuous free gas phase.

On the other hand, kinetic models have also been introduced and implemented in thermal reservoir simulators that allow chemical reactions to be explicitly defined (CMG-STARS, 2016). Their main thesis is that a dispersion of tiny bubbles in a continuous oil phase is not a thermodynamically stable species. Provided that the conditions are met (i.e., time and pressure environment), this dispersion will separate into the two distinctive phases: gas and oil. Not only does this approach account for the time-dependent behavior of foamy oil, but also the impact of imposed flow conditions (i.e., regeneration of dispersed bubbles is possible even after phase segregation). Coombe and Maini (1994) developed a model that describes the morphology of the gas-in-oil dispersion. Basically, three components are defined: dead oil, dissolved gas, and

dispersed gas (bubbles). The dissolved gas changes to dispersed gas, and this one transitions to free gas by means of rate processes with associated rate constants. This model is not considered useful for forecasting the influence of various operating conditions as it fails to consider the influence of time and the position-dependent capillary number (Maini, 2001).

2.2 Post-CHOPS

Primary recovery of heavy oils necessarily involves the decline of reservoir pressure, and when this value is low enough (in a range of 250 to 1,000 kPa depending on the fluid and reservoir depth), oil production drops to uneconomic rates leaving more than 85% of the reserves in place (Dusseault, 2007). Heavy oil is conventionally produced by enhanced oil recovery (EOR) methods such as water injection (with added polymers or viscosifying agents), solvent injection, and thermal approaches. Thermal methods are the preferred approach due to the imperative need to improve the mobility of heavy oil at reservoir conditions. An increase in temperature is known to contribute to the drainage process by reducing the viscosity and therefore mobilizing the oil to the wellbore.

2.2.1 Conventional EOR Approaches for Heavy Oil Recovery

Waterflooding is not particularly a very attractive approach to increase the recovery factor from heavy oil deposits due to the viscosity difference between the in-situ fluid and the injected water. This creates an adverse mobility ratio that often leads to water fingering, causing early breakthrough and therefore, reducing the total effectiveness of the water-drive.

Despite of these negative consequences, some successful applications have been recorded in the Captain Field (North Sea), where horizontal wells are used for both water injection and heavy oil production. These horizontal water injectors provide a better distributed pressure maintenance system as well as an effective line-water drive (Speight, 2009). Polymer-augmented water injection has also been identified as a potential recovery option due to the increased viscosity of the injection fluid and the improvements in its mobility control.

Thermal approaches are, without doubts, the preferred approach for heavy oil recovery. The successful implementation of steam-assisted gravity drainage (SAGD) in Western Canada and Venezuela have encouraged operators from all over the world to consider this well pair setup in their recovery projects. Continuous steam injection and steam huff & puff are also common in the industry due to a reduction in oil viscosity once the hot steam/water transfers heat to the in-situ fluid, helping to mobilized it to the wellbore.

Numerous non-thermal methods, including vapor extraction (VAPEX), solvent flooding, cyclic solvent injection (CSI), enhanced cyclic solvent process (ECSP), and cyclic CO_2 treatment, are other alternatives that have been successful in terms of increasing the recovery of heavy oil.

These approaches, however, have to be carefully selected on a reservoir-by-reservoir basis, which means that any practice proven to be successful in a given reservoir might not necessarily be the best approach to be implemented in another reservoir. This is usually the case for post-CHOPS reservoirs, in which the geological characteristics (i.e., thin pays and wormhole networks) introduce a big challenge in terms of operational strategies and numerical simulation studies.

In the case of waterflooding, the presence of high-permeability channels in the reservoir leads to early water breakthrough as the injected liquid will preferentially flow through these networks bypassing the in-situ heavy oil. In terms of thermal applications, considering the fact that many CHOPS reservoirs are quite thin with low net pays, typically less than 10 m, (Du et al., 2015), thermal methods are not considered effective due to excessive heat loss, which renders the scheme uneconomic. In a similar way, the main driving force in a VAPEX process is gravity, which may be insufficient in thin deposits (Yadali Jamaloei, 2013). Continuous solvent injection processes are also inefficient since the high-permeability wormholes may cause the solvent to bypass the in-situ oil leading to early solvent breakthrough, similar to what it is observed in waterfloodings.

2.2.2 Preferred EOR Approaches for Post-CHOPS

In contrast, the wormhole network plays a beneficial role in a cyclic solvent injection (CSI) process by exposing a larger contact area between the solvent and heavy oil (Chang and Ivory, 2013) and giving more reservoir access to the solvent to reach other areas located far away from the wellbore. Simultaneously, it also provides flow channels for the diluted oil to flow back to the wellbore (Du et al., 2015). Therefore, cyclic solvent injection (CSI) is widely recognized and accepted as be the most promising follow-up technique for post-CHOPS production.

A typical single-well cyclic injection process CSI process entails multiple cycles, with each cycle consisting of 3 stages: injection, soaking, and production. During the injection stage, a light hydrocarbon solvent is injected at high pressure; the well is subsequently closed during the soaking period, during which the solvent dissolves into the oil to reduce the oil viscosity, and the

fluid pressure gradually decreases (Yadali Jamaloei et al., 2015). The well is finally reopened, and the diluted oil flows back to the wellbore.

2.2.3 Field Experiences

Cyclic solvent injection (CSI) strategies, using the Huff & Puff principle (i.e., injection, soaking, and production), have been subject to extensive laboratory studies and pilot testing (Chang and Ivory, 2013). Wormhole networks contribute by increasing the contact area and enhancing the mixing between the solvent and the heavy oil. Diluted oil would migrate to areas around the wellbore, where it can be drained more efficiently.

Some operators in the Canadian province of Saskatchewan have piloted cyclic solvent approaches. In particular, Nexen and Husky have been pioneers in this field by carrying out field-scale pilot tests. The Joint Implementation of Vapour Extraction (JIVE) project, supported by the Petroleum Technology Research Centre (PTRC), ran from 2006 through 2010, and it was considered to be the first field-scale application of solvent-based schemes in post-CHOPS reservoirs (Chang and Ivory, 2013).

2.3 Modeling of Post-CHOPS Applications

2.3.1 Common Approaches

Numerical simulations are necessary in order to perform proper assessments of pilot or field-scale post-CHOPS applications. However, since the modeling scale is typically much larger than the wormhole's size, incorporating lab-scale physics is not trivial. In the end, it is necessary to quantify the effects of heterogeneities below the modeling resolution for realistic predictions with these numerical models.

A graphic illustration of the most commonly-used modeling approaches is presented in Fig 2.5. Some authors have proposed the use of an effective high-permeability zone to represent the regions where wormholes have been formed as seen in Fig 2.5 (a) (Chang and Ivory, 2013; Sun, 2012).

Dual-permeability approaches are also common, where the wormhole network is represented as fractures, as shown in Fig 2.5 (b) (Rangriz-Shokri, 2015). Model parameters are often assigned in a manner that violates the realistic spatial variation in wormhole characteristics: for example, shape factor, fracture porosity, and dispersivity are assigned uniformly in such a way that it does not represent the actual complexities in terms of heterogeneity (i.e., blocks have different wormhole intensity).

Another approach is to define a dilated zone around the well, in which much higher porosity and permeability values are set [Fig. 2.5 (c)]. Finally, wormholes can also be represented as extended wellbore sections [Fig. 2.5 (d)]; different wellbore diameters, which are often estimated via history matching of oil/sand production data, would be assigned in the main and secondary branches.

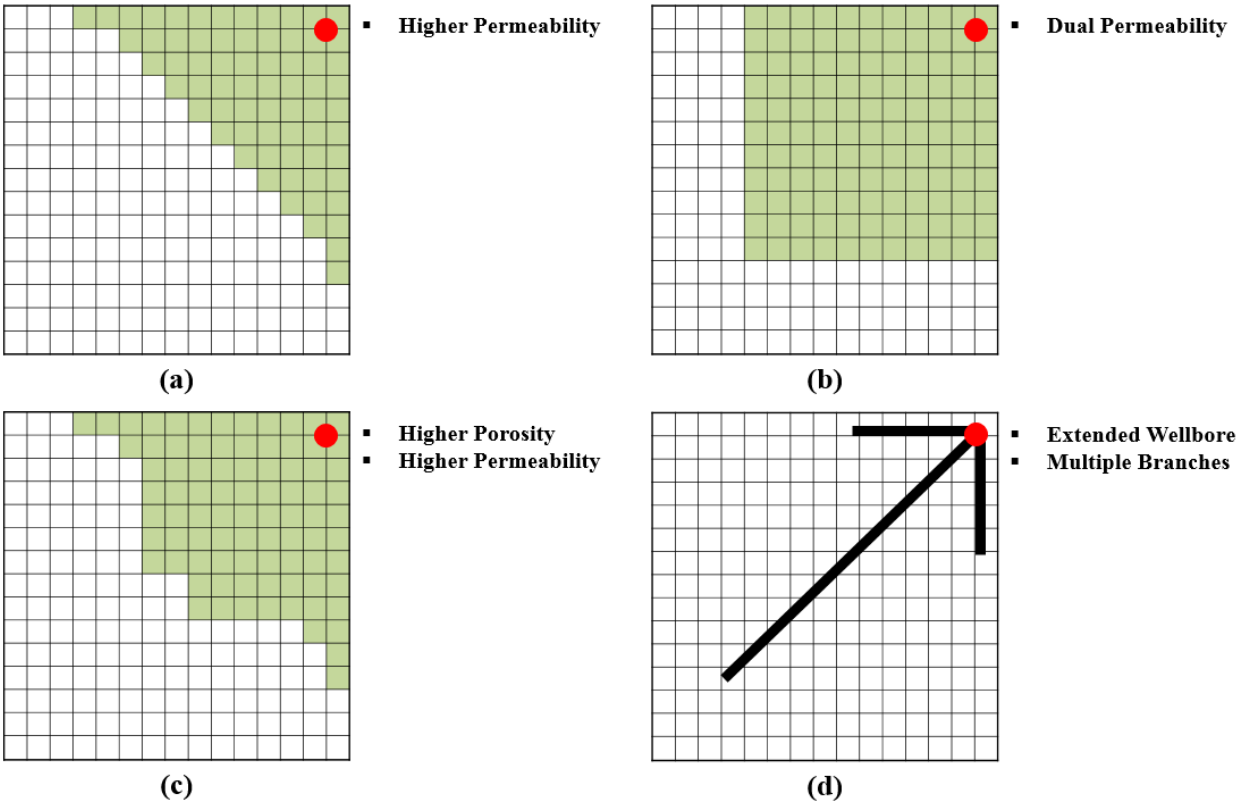

Fig. 2.5 – Commonly-used approaches to model wormhole networks

(a) High-permeability zone; (b) Dual-permeability; (c) Dilated zone; (d) Extended wellbore branches

One of the main issues recently identified (Chang and Ivory, 2013) is the impact of upscaling (i.e., the use of larger grid blocks instead of fine ones) on the recovery response of these approaches.

Although many of these modeling approaches have been published and used in the past, there remains a lack of systematic workflow for conditioning these numerical models against lab-scale measurements and representing wormholes that span over multiple physical scales.

Representing the realistic spatial variation in wormhole characteristics is key to capturing the actual interactions occurring at the fine scale.

Liu and Zhao (2005) introduced a diffusion-limited aggregation (DLA) algorithm to model wormhole networks as fractal patterns. This approach may not depict the precise configuration of these complex wormhole networks, but it is considered to be an acceptable mathematical approximation to the complex characteristics of the wormhole channels. Fig. 2.6 illustrates four different realizations of wormholes networks using a fractal approach by means of a diffusion-limited aggregation (DLA) algorithm. Note that the patterns keep the fractal characteristics consistently (i.e., main branches also exhibit branching and so do sequential branches).

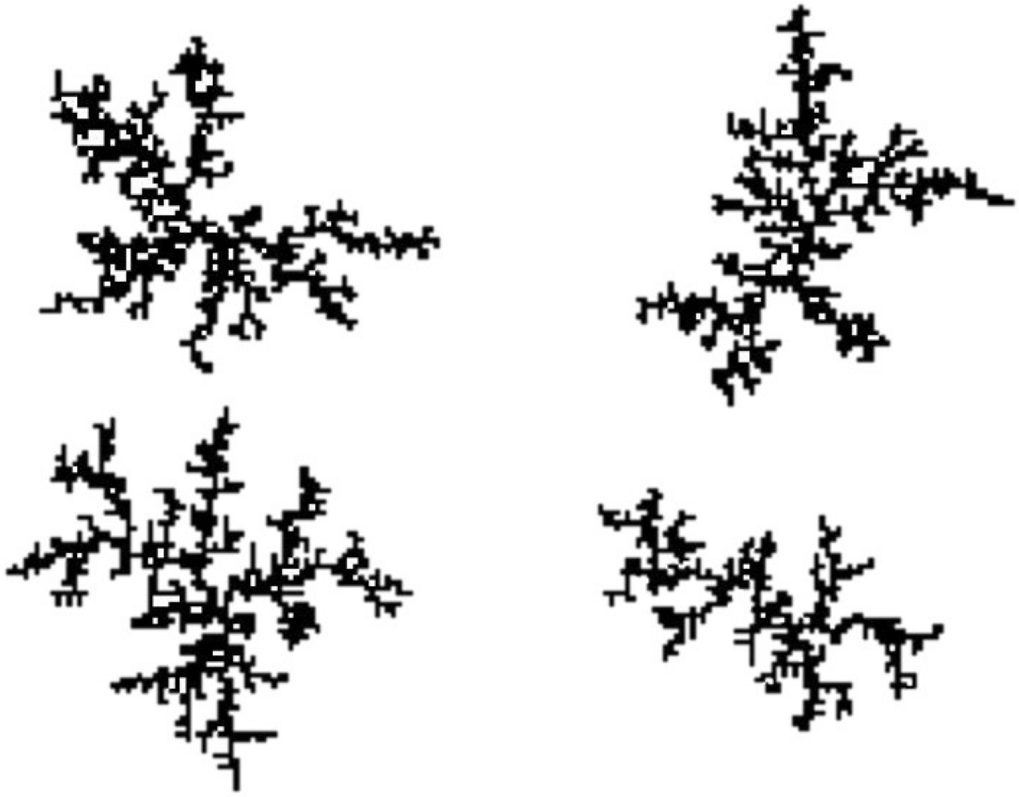

Fig. 2.6 – Multiple realizations of wormhole networks using a fractal approach

The main issue with performing flow simulations at the field scale with these high-resolution wormhole models is the computation cost. Thousands of simulations cells would be necessary to explicitly model these complex networks in a compositional simulator, which alone requires more computational power than a conventional black-oil simulator.

2.3.2 Pitfalls/Shortcomings in Current Models

For cyclic solvent injection processes, solvent and oil transport is a combined result of advection and molecular diffusion, which can be further enhanced by dispersion caused by heterogeneities occurring at various scales, such as those complex distributions of wormholes. Both longitudinal and transverse dispersivities tend to increase with scale and heterogeneity (Vishal and Leung, 2015).

The success of these processes often depends on the ability of the solvent to contact the oil. Numerical simulations are needed for analysis of pilot or field-scale applications. The ability to extrapolate lab-scale measurements to the simulation modeling scale is extremely important, since these processes require the solvent to get from the wormhole into the oil, and diluted oil to drain faster than solvent can evolve with dropping pressure. However, since the modeling scale is typically much larger than the wormhole's size, incorporating lab-scale diffusion data (which often neglects the effects of wormholes) is not trivial. In the end, it is necessary to quantify the effects of heterogeneities below the modeling resolution for realistic predictions with these numerical models.

Common field-scale simulations are performed with a minimum grid block size of 1 to 5 m. Due to the lack of systematic workflow for conditioning these numerical models against lab-

scale measurements and representing wormholes that span over multiple physical scales, values of fracture spacing, shape factor and dispersivity are often assigned in a manner that ignores the spatial variation in wormhole characteristics: for example, assuming uniform values everywhere in the domain (Rangriz-Shokri, 2015). History matching is usually conducted via arbitrary adjustment of dispersivity, without accounting for the varying wormhole distribution.

Chapter 3: Methodology

3.1 Overview

A practical and easy-to-implement scale-up workflow is proposed in order to estimate the properties of the equivalent coarse-scale dual-permeability continuum model. The following steps are involved in the development of this framework:

1. Heavy oil phase behavior is modeled using the Peng-Robinson equation of state and some parameters are adjusted via regression analysis in order to match the experimental observations. Foamy oil flow is modeled using the modified fractional-flow approach, which involves adjusting the gas relative permeability functions to approximate the actual recovery response. Two sets of relative permeability curves are used: one for the injection and soaking stages and another one for the production stage (with reduced gas relative permeability end point and higher irreducible gas saturation).

2. A set of high-resolution (fine-scale) simulation models exhibiting different wormhole configurations are constructed. Both matrix and high-permeability wormholes are represented explicitly in the computational domain, such that flows of solvent and oil in the matrix and wormholes can be directly simulated. It is currently assumed that the wormholes are fully developed and growth of wormhole networks can be ignored (a reasonable assumption for post-CHOPS applications). Additional physical mixing due to

heterogeneities in the matrix can be approximated with an increase in dispersivity. The extent of numerical (artificial) dispersion is controlled using higher-order flux approximation schemes.

3. Effective or scaled up dual-permeability models at different averaging scales are computed. A "flow-based" scale-up approach is adopted, by which the difference in recovery response (i.e., profiles of oil/gas production) between the detailed model and the equivalent dual-permeability continuum model is minimized. In the end, bivariate distributions of effective longitudinal/transverse dispersivities are constructed as functions of wormhole intensity. They are subsequently used in a cloud transform procedure to construct models of effective dispersivities for larger field-scale simulations.

3.2 Fluid Model

Phase behavior is modeled based on the fluid composition analysis of a typical Canadian heavy oil sample presented in Yadali Jamaloei (2013). The detailed fluid composition measured at the Saskatchewan Research Council (SRC) is presented in Table 3.1. The Peng-Robinson Equation of State (EOS) is used to model the experimental behavior of the fluid, which requires certain parameters such as critical pressure, critical temperature, and acentric factor to be tuned via regression analysis to match PVT experimental observations (i.e., saturation pressure and viscosity profile). The experimental measurements are presented in Table 3.2 and Fig. 3.1

illustrates the experimental and predicted behavior of saturation pressure and viscosity after tuning the equation of state.

Component lumping is implemented in order to reduce the number of calculations to be performed by the compositional simulator. The lumping scheme and the resulting tuned critical properties and acentric factors are presented in Table 3.3.

Flash calculations of methane-propane and dead oil mixtures are performed and the corresponding predictions are compared with those presented in Yadali Jamaloei (2013) as a way to validate the numerical PVT model and approximate the behavior of the mixtures in a gas solvent injection scheme.

Table 3.1 – Fluid composition analysis

[Adapted from Yadali Jamaloei (2013)]

Component	Mole %	Component	Mole %
C1	0.00	C23	2.11
C2	0.00	C24	1.82
C3	0.00	C25	1.91
IC4	0.30	C26	1.67
NC4	0.50	C27	1.65
IC5	1.25	C28	1.53
NC5	0.89	C29	1.44
C6	1.58	C30	1.30
C7	0.00	C31	1.24
C8	0.00	C32	1.27
C9	2.99	C33	0.87
C10	4.71	C34	0.89
C11	4.04	C35	1.13
C12	4.24	C36	1.08
C13	4.66	C37	0.69
C14	4.25	C38	0.71
C15	4.49	C39	1.16
C16	3.69	C40	1.12
C17	3.54	C41	0.61
C18	3.60	C42	0.58
C19	3.03	C43	1.02
C20	2.68	C44	0.65
C21	2.84	C45	0.63
C22	1.86	C46+	17.78

Table 3.2 – Experimental measurements

[Adapted from Yadali Jamaloei (2013)]

Feed Methane Mole Fraction	Saturation Pressure (kPa)	Oil Viscosity (mPa*s)
0.1040	2,000	1,380
0.1566	4,000	930
0.2402	6,000	622
0.3018	8,000	424

Table 3.3 – Fluid properties after component lumping and regression

Component	Molar Fraction	Pc (atm)	Tc (K)	Acentric Factor
CH4	0.000	45.400	190.600	0.008
C3H8	0.000	41.900	369.800	0.152
IC4-C14	0.296	23.769	633.436	0.465
C15-C30	0.394	14.089	676.470	0.837
C31-C45+	0.310	6.236	871.310	1.363

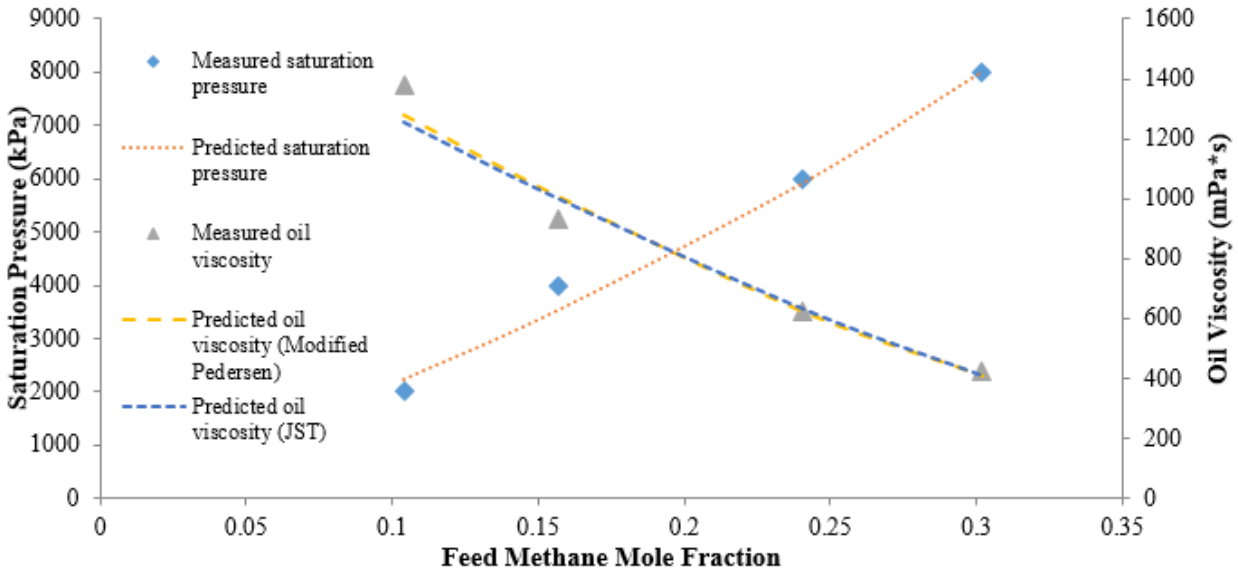

Fig. 3.1 – Experimental measurements vs. predicted behavior

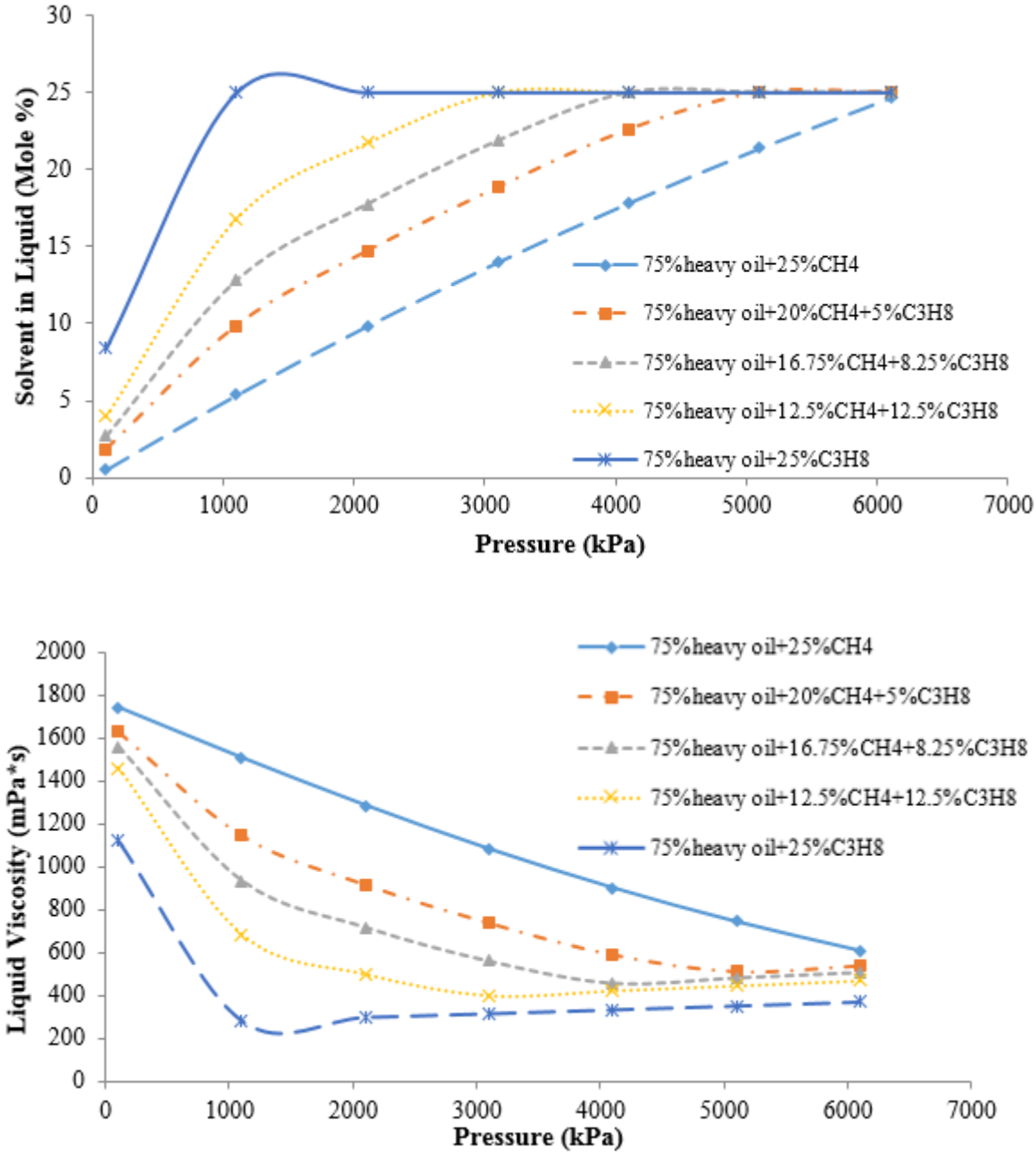

Fig. 3.2 – Flash calculations plots

Solvent in liquid (top); Liquid viscosity (bottom)

Live oil condition is approximated by injecting a mixture of methane and propane in equal molar fractions (i.e., 50% C1 and 50% C3) until a typical field producing gas-oil ratio (GOR) of 15 sm^3/m^3 is achieved. The live oil properties of the recombined sample (dead oil + gas) is presented in Table 3.4.

Solvent injection processes typically use carbon dioxide (CO_2) or a mixture of light hydrocarbons components (e.g., methane, ethane, and propane). The molar composition of the solvent mixture used for this study is 60% of methane and 40% of propane. This optimal methane/propane ratio is highly dependent on the in-situ heavy oil properties; therefore, a sensitivity analysis is recommended in order to find the optimal combination that renders the best recovery response.

Table 3.4 – Live oil fluid properties after recombination

Component	Molar Fraction	Pc (atm)	Tc (K)	Acentric Factor
CH4	0.1153	45.400	190.600	0.008
C3H8	0.1153	41.900	369.800	0.152
IC4-C14	0.2278	23.769	633.436	0.465
C15-C30	0.3034	14.089	676.470	0.837
C31-C45+	0.2382	6.236	871.310	1.363

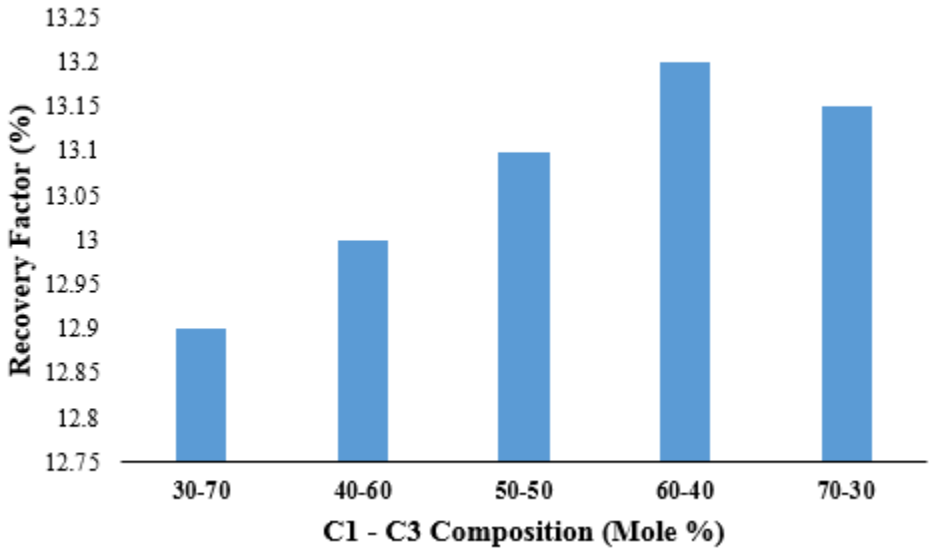

Fig. 3.3 – Oil recovery for different combinations of methane-propane

3.2.1 Foamy Oil Model

The modified fractional-flow approach is adopted to represent the enhanced oil flow and delay of free gas flow due to foamy oil behavior. This is achieved by assigning a lower gas relative permeability end point, which is accompanied by higher irreducible gas saturation, during the production stage. The relative permeability functions for the matrix and wormhole during the injection/soaking stages are presented in Fig. 3.4, while the modified relative permeability functions for the matrix and wormhole during the production stage are illustrated in Fig. 3.5. Note the higher irreducible gas saturation and the lower end point of the gas function.

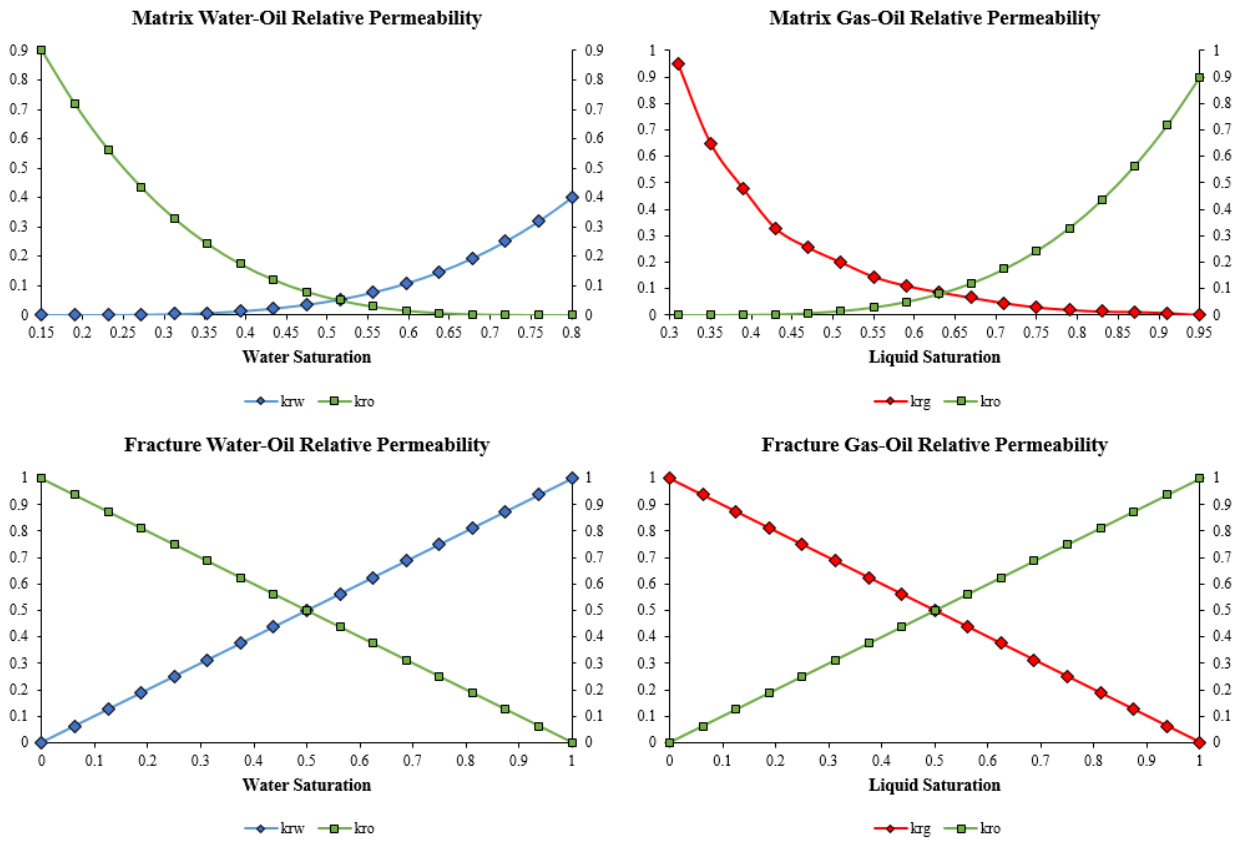

Fig. 3.4 – Relative permeability functions for injection and soaking

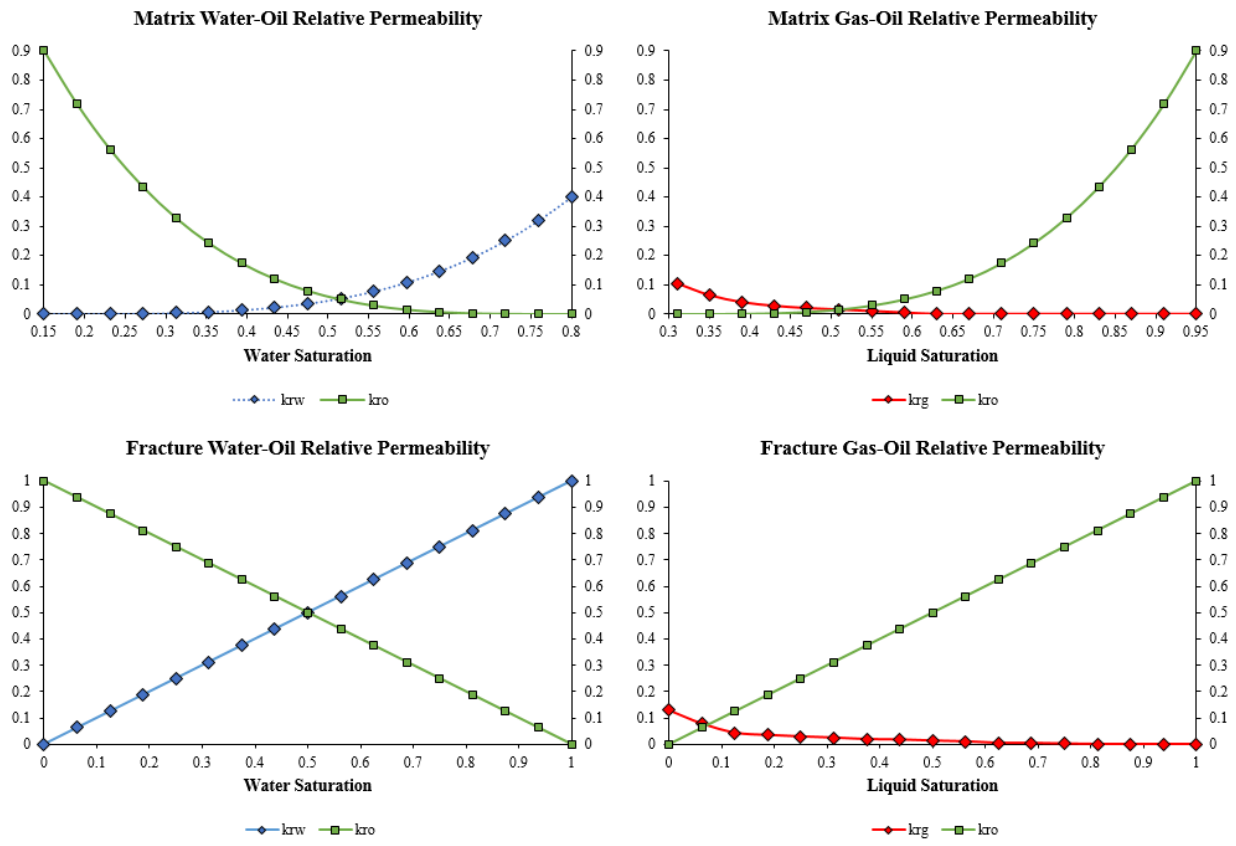

Fig. 3.5 – Relative permeability functions for production

3.3 Fine-Scale Models

A series of fine-scale three-dimensional compositional models in the Cartesian coordinates are constructed. The model consists of 120 × 120 × 5 grid blocks ($\Delta x = 0.25$ m; $\Delta y = 0.25$ m). The dimensions of the entire model are 30-meter wide, 30-meter long, and 1-meter thick. It is assumed that the wormhole network is confined in the middle layer; therefore, $\Delta z = 0.25$ m in the middle layer. The grid size along the z-direction in the over/underlying layers is computed according to Eq. 3.1, which represents a logarithmic thickness refinement:

$$T_i = \frac{T_{WH}}{2} \exp\left[\frac{2i}{N-1} \ln\left(\frac{2T_{HALF}}{T_{WH}} \right) \right] \quad \text{Eq. (3.1)}$$

Where T_{WH} denotes the thickness of the wormhole plane, i is the index of any individual layer, N is the total number of layers, T_{HALF} is the half of the entire thickness, T_i is then the distance from the outer boundary of layer i to the center of the wormhole plane.

Logarithmic thickness refinement is especially useful for improving the stability of the numerical solution when high size contrast between adjacent grid blocks is present. The resulting thickness corresponding to each layer is summarized in Table 3.5.

Table 3.5 – Thickness of each layer computed using logarithmic refinement

Layer	Thickness (m)
1st	0.2386
2nd	0.1364
3rd (Wormhole)	0.2500
4th	0.1364
5th	0.2386

Due to the uncertainty in the actual wormhole configuration, a deterministic modeling of the wormhole network is nearly impossible due to the unknown subsurface distribution of these complex structures and the difficulty in gathering reliable data (e.g., seismic methods) to

delineate their precise configurations. Statistical approaches may offer a viable alternative to characterize the wormhole networks. Following the diffusion-limited aggregation (DLA) algorithm (Liu and Zhao, 2005), a series of fractal patterns representing networks of wormholes extending in a 30 meters by 30 meters two-dimensional space is constructed. The fractal pattern grows around the wellbore, which happens to be the geometrical center of the model. The sizes of these network branches should closely approximate typical experimental and field observations; for instance, the wormhole diameter is larger in near-wellbore region, and it gradually decreases towards the tip of each branch).

These multiple realizations of two-dimensional fractal patterns are represented in a binary form. Each fractal pattern is then converted to a wormhole network: blocks with a value of 1 belong to the wormhole network, and blocks with a value of 0 represent matrix [Fig. 3.6 (a)]. A top view of the middle layer that contains the wormhole network, as well as the side view of the model, are shown in Fig. 3.7 (a) and (b), respectively. Considering the spatial aggregation of wormhole blocks, a range of wormhole diameter between 25 cm to 50 cm is obtained, which is consistent with field observations in Chang and Ivory (2013).

Porosity and permeability for the matrix are derived from averages of several UCSS reservoirs in Saskatchewan. Higher porosity and permeability values are assigned to the wormhole blocks. Table 3.6 summarizes the main model attributes. In this study, additional sub-grid heterogeneities in the matrix are not considered; therefore, dispersivity is set to zero in the fine-scale model.

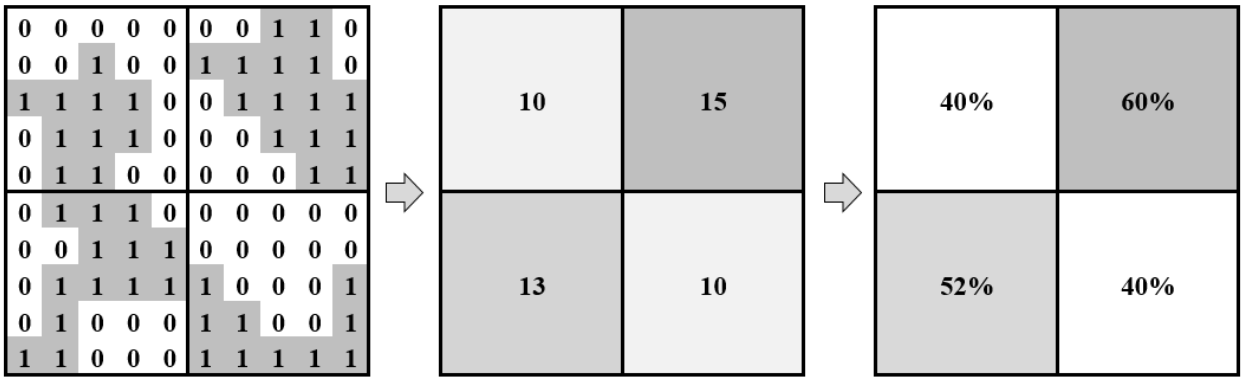

Fig. 3.6 – Binary representation and characterization of wormhole networks

(a) Binary system; (b) Number of wormholes in each coarse-scale grid block; (c) Wormhole intensity in each coarse-scale grid block

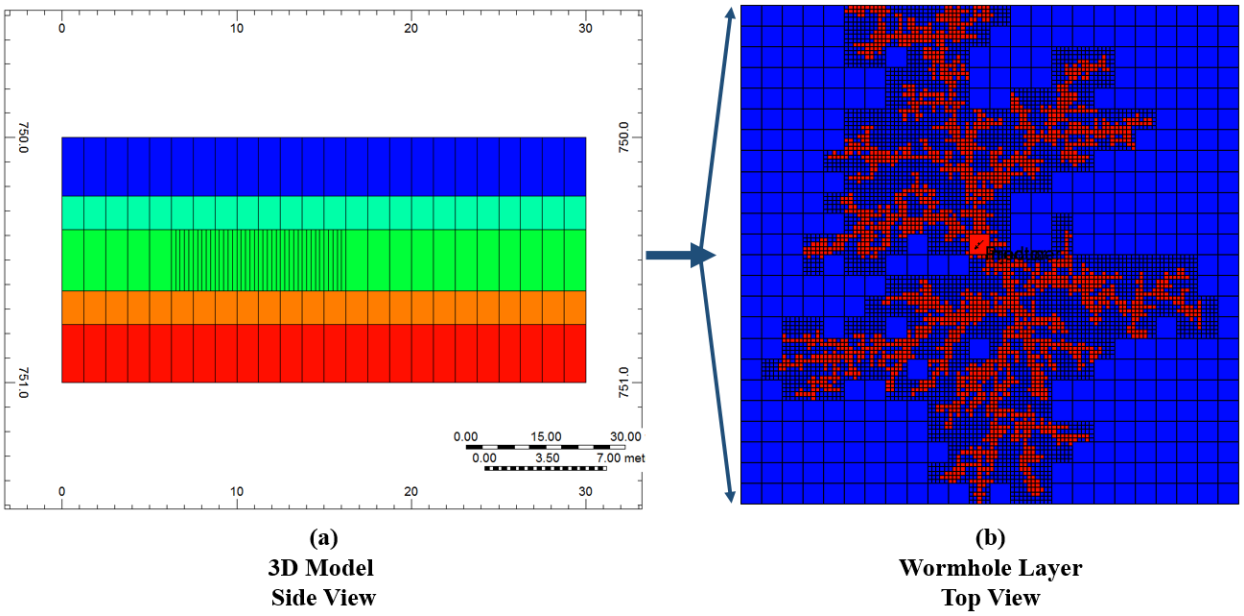

Fig. 3.7 – Fine-scale model

(a) Side view of the model; (b) Wormhole layer

Table 3.6 – Model attributes

Parameter	Units	Value
Depth	m	750
Thickness	m	1
Reservoir Pressure	MPa	2
Reservoir Temperature	Celsius	20
Wormhole Porosity	Fraction	0.60
Matrix Porosity	Fraction	0.30
Wormhole Permeability	Darcy	60
Matrix Permeability	Darcy	3
Operating Conditions	**Units**	**Value**
Injection Composition		
CH4	mol/mol	0.60
C3H8	mol/mol	0.40
Diffusion Coefficient	cm^2/s	0.001
Production Schedule	**Units**	**Value**
Injection Rate	m^3/day	25
Injection Time	Day	20
Soaking Time	Day	10
Production Pressure (BHP)	MPa	1

The model is initialized to approximate the conditions commonly encountered at the end of a typical CHOPS operation. Assuming a typical recovery factor of approximately 12% at the end of CHOPS (Soh, 2016), the fluid saturations are then explicitly assigned in such a way that the oil saturation in the matrix would gradually decrease with proximity to the depleted wormholes (typically referred to as the depletion envelop). Fig. 3.8 illustrates the initial oil saturation distribution (end of CHOPS) corresponding to one of the realizations for post-CHOPS modeling. An initial pressure of 1,000–2,000 kPa is commonly observed in the field at the end of CHOPS operation (Chang and Ivory, 2013).

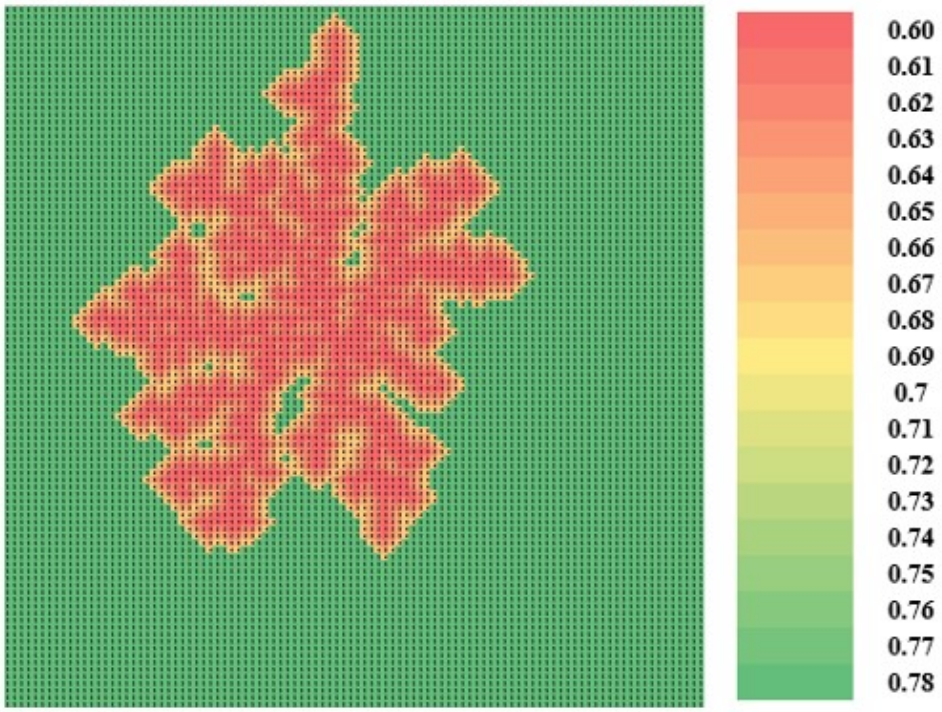

Fig. 3.8 – Typical oil saturation distribution at the end of CHOPS

Operational constraints, such as solvent injection rate, type of solvent, and duration corresponding to each one of the three stages in a typical cyclic solvent injection process are scaled down from field practices to the model scale (Rangriz-Shokri, 2015). For instance, for the injection stage, the injection rate is adjusted such that the total pore volume injected is comparable to values reported in field/pilot applications; common practice usually entails an injection period that continuously spans over 20 days, which is followed by 10 days of soaking period. Finally, the well is brought on production by slowing decreasing the bottomhole pressure (a 30-100 kPa/day depletion scheme is commonly used in the field). The terms "fine-scale model" and "wormhole case" will be used interchangeably.

3.4 Coarse-Scale Models

A dual-permeability approach is employed to facilitate the scale-up process. Two systems are defined in this approach: matrix and fracture systems, with the latter representing the wormhole network. Different from the conventional dual-porosity system, a dual-permeability approach allows flow between adjacent matrix blocks. Fig. 3.9 presents a graphical comparison between the dual-porosity and dual permeability systems. Although the dual-permeability approach is more expensive in terms of computational effort, it provides a more realistic approach to modeling the actual interactions between the injected solvent and the in-situ heavy oil in the matrix. The terms "coarse-scale model" and "dual-permeability case" will be used interchangeably.

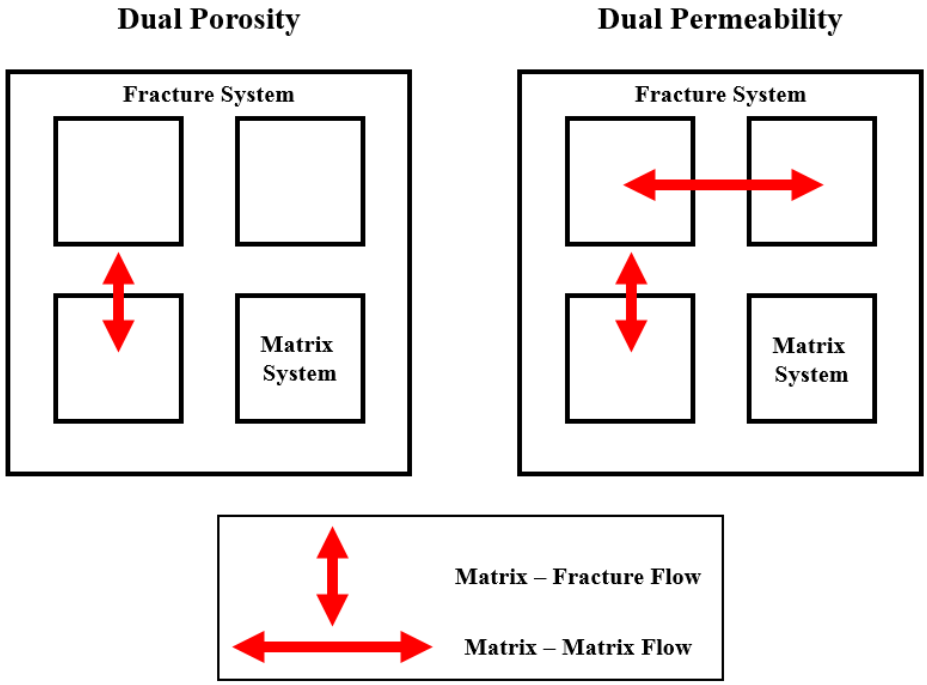

Fig. 3.9 – Illustration of flows in Dual-Porosity and Dual-Permeability systems

Corresponding to each fine-scale model generated in section 3.3, an equivalent coarse-scale three-dimensional compositional model is constructed. The model consists of 24 × 24 × 1 grid blocks (Δx = 1.25 m; Δy = 1.25 m; Δz = 1 m). The dimensions of the entire model are 30-meter wide, 30-meter long, and 1-meter thick (same as the fine-scale model). Each grid block in the coarse-scale model is the equivalence of 75 fine-scale grid blocks. The dimensions of the coarse blocks are Δx = 1.25 m, Δy = 1.25 m, and Δz = 1 m respectively. Fig. 3.10 illustrates a comparison of fine-scale and coarse-scale grid blocks.

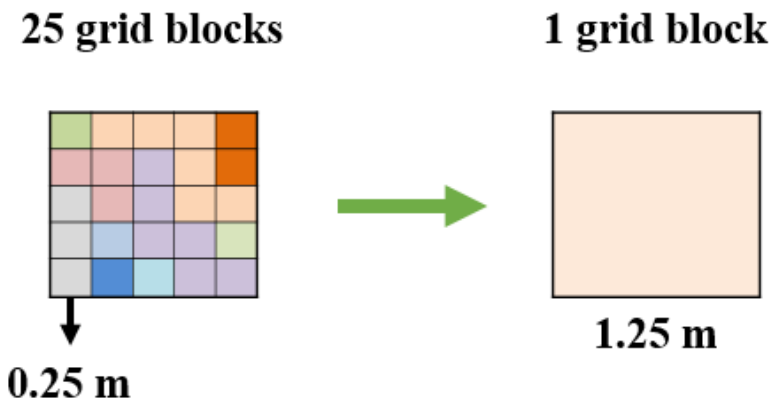

Fig. 3.10 – Fine-scale vs. coarse-scale

Fracture and matrix porosities in the coarse-scale (dual-permeability) model, $Ø_{F(DK)}$ and $Ø_{M(DK)}$, are computed via volume-weighted linear averaging using Eq. 3.2 and Eq. 3.3, respectively:

$$\phi_{F(DK)} = \frac{V_{WH}\phi_{WH}}{V_{coarse}} \qquad \text{Eq. (3.2)}$$

$$\phi_{M(DK)} = \frac{V_{M}\phi_{M}}{V_{coarse}} \qquad \text{Eq. (3.3)}$$

Where V_{coarse} denotes the bulk volume of the coarse-scale block; V and Ø denote volume and porosity, respectively, while the subscripts "WH" and "M" denote wormhole and matrix properties, respectively. The shape factor (σ) is another parameter required to fully describe dual-permeability systems. It is needed to compute the fluid transfer between the matrix and the

fracture systems. According to the formulation introduced by Gilman and Kazemi (1983), as presented in Eq. 3.4:

$$\sigma = 4\left(\frac{1}{L_x^{\,2}} + \frac{1}{L_y^{\,2}} + \frac{1}{L_z^{\,2}}\right) \qquad \text{Eq. (3.4)}$$

Where L_x, L_y, and L_z denote the fracture spacing along the x-, y-, and z- direction, respectively. Given that shape factor is multiplied with the interfacial area of a given grid block to represent the total contact area between the matrix and fracture systems, it is calculated based on the actual contact area between all the matrix and the wormhole cells in the fine-scale model for each coarse-scale grid block. A uniform fracture spacing ($L_x = L_y = L_z$) is chosen in such a way that they would reproduce the same matrix-wormhole contact area as in the fine-scale model.

Finally, to compute the bivariate relationships between wormhole intensity (WI) and effective dispersivities for the dual-permeability system, a flow-based technique is adopted. First, WI is computed for each coarse-scale grid block: $WI = V_{WH}/V_{coarse}$ [Fig. 3.6 (c)]. Since WI would vary spatially (e.g., WI decreases away from the well), three bins of WI values are considered: high wormhole intensity ($WI \geq 60\%$), medium wormhole intensity ($30\% < WI < 60\%$), and low wormhole intensity ($WI \leq 30\%$). An objective function, in terms of mismatch in the cumulative oil and gas production profiles between the fine-scale model and the equivalent coarse dual-permeability system, is defined. Longitudinal and transverse dispersivities (α_L and α_T) in both the fracture and matrix systems, corresponding to each bin, are tuned to minimize the

mismatch. This step is implemented using CMG's C-MOST (CMG-CMOST, 2016) for all fine-scale models constructed in sections 3.3 and 3.4.

Multiple random realizations of the wormhole networks (30 m × 30 m) generated with the diffusion-limited aggregation (DLA) algorithm are illustrated in Fig. 3.11. All these wormhole networks have similar overall areal coverage, which is approximately 12% of the entire layer in which each network is explicitly modeled (this corresponds to a 2.3% volumetric coverage over the entire pay thickness, as reported in most field operations).

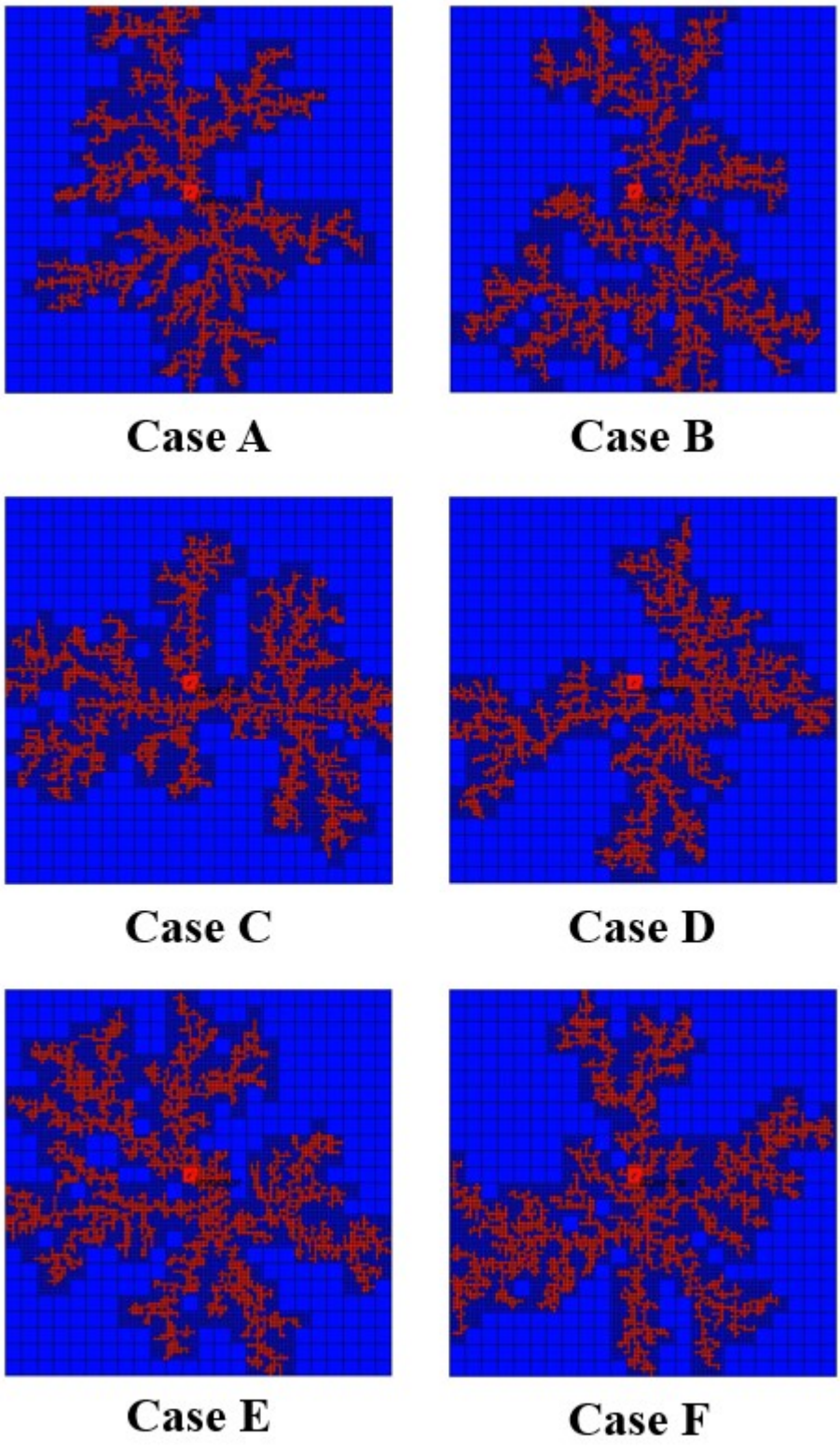

Fig. 3.11 – Multiple wormhole networks used for calibration

In the end, distributions of effective dispersivities corresponding to different categories of wormhole intensity, i.e., $P(\alpha_L,i|WI)$ and $P(\alpha_T,i|WI)$, are constructed (i = matrix, fracture). This step is facilitated by fitting a distinctive Gaussian function corresponding to the set of effective dispersivity values in each bin. The entire scale-up workflow is summarized in Fig. 3.12. The calibrated bivariate distributions are used in a cloud transform procedure to construct models of α_L and α_T, which are correlated to WI (wormhole intensity), at the field scale (considering a grid size that is the same as the coarse block). This means assigning effective dispersivities at each location by sampling from $P(\alpha_L,i|WI)$ and $P(\alpha_T,i|WI)$ according to the WI value/bin at that particular location (Vishal and Leung, 2015). In this study, values are sampled from the series of Gaussian functions obtained from the aforementioned scale-up analysis.

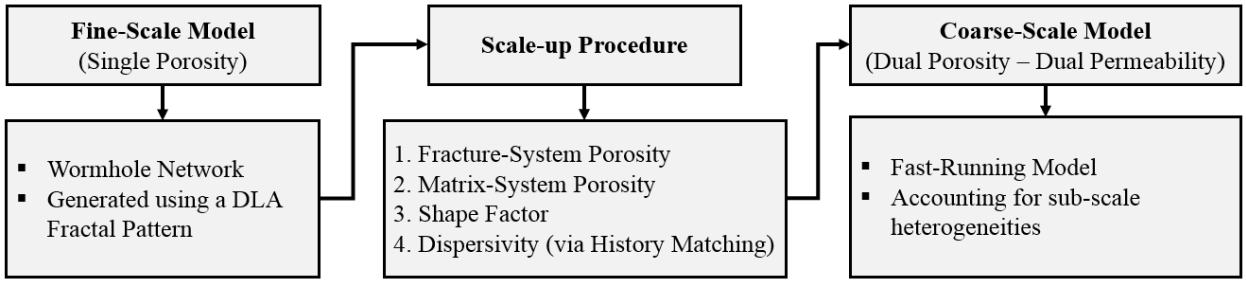

Fig. 3.12 – Summary of the scale-up workflow

As an example, 7 realizations of the fine-scale models are constructed, and the coarse-scale dispersivity values for both fracture and matrix systems corresponding to each WI level are summarized in Table 3.7. These values are also plotted in Fig. 3.13 and Fig. 3.14. It is observed that as wormhole intensity increases, fracture dispersivity also increases. This reflects the additional mixing as a result of variation in flow paths among the wormholes. On the other hand,

as wormhole intensity increases, the contribution to solvent transport from matrix dispersion is less prominent, since less matrix volume is remaining in a bulk grid block. Therefore, a decreasing trend in matrix dispersivity with wormhole intensity is observed. Fig. 3.15 shows the fitted Gaussian distributions of effective dispersivity in the fracture and matrix systems for different levels of wormhole intensity (WI). Fig. 3.16 illustrates the cumulative distribution functions (CDF) of the Gaussian bivariate distributions respectively.

Table 3.7 – History-matched dispersivities for the matrix and fracture systems

		Wormhole Intensity		
		High	**Medium**	**Low**
		60-100%	**30-60%**	**0-30%**
Case A	Fracture	4.8875	3.1500	0.9525
	Matrix	0.9725	2.6100	5.5000
Case B	Fracture	4.2000	1.5050	0.9850
	Matrix	0.7725	1.6650	3.6900
Case C	Fracture	4.3500	1.9450	1.0500
	Matrix	1.1850	1.5500	3.5300
Case D	Fracture	4.1700	2.1000	0.8275
	Matrix	0.8050	2.3700	3.9600
Case E	Fracture	3.8500	1.6650	0.8375
	Matrix	0.9900	1.8800	3.4500
Case F	Fracture	3.2000	2.5000	0.8000
	Matrix	0.8000	2.3000	3.4000
Case G	Fracture	4.8200	2.2350	0.8750
	Matrix	0.9200	2.1800	4.7700

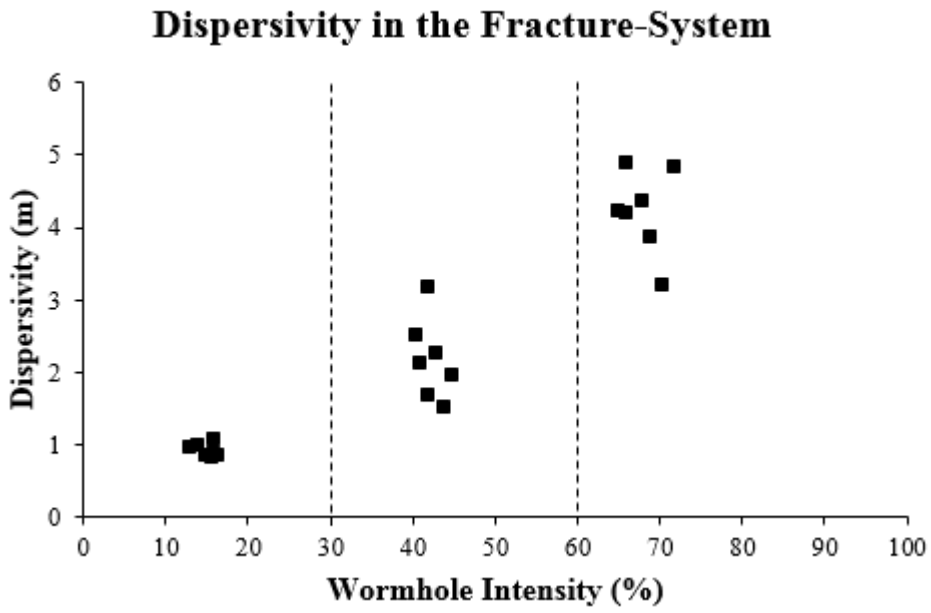

Fig. 3.13 – Bivariate distribution of WI and Dispersivity ($\alpha_L = \alpha_T$) in the Fracture

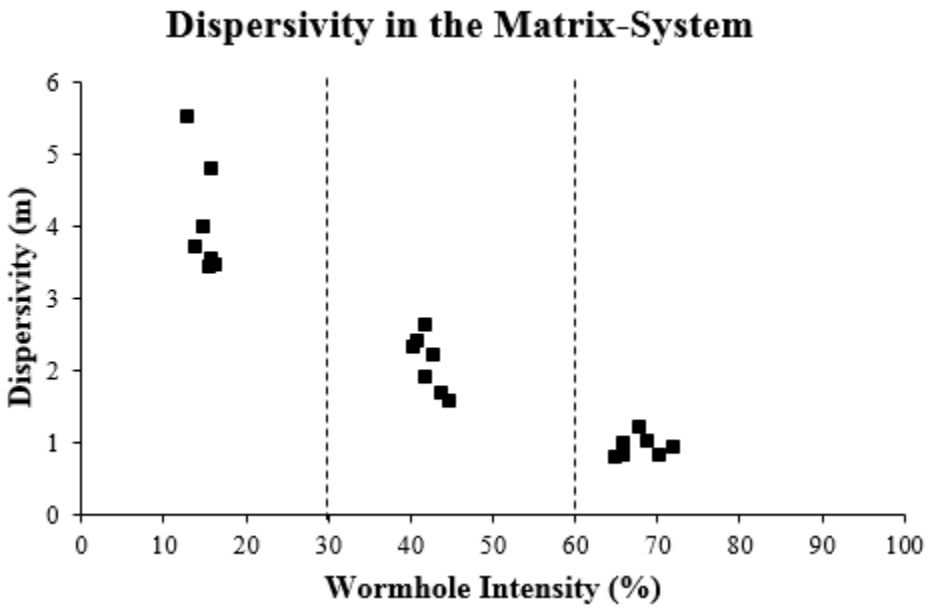

Fig. 3.14 – Bivariate distribution of WI and Dispersivity ($\alpha_L = \alpha_T$) in the Matrix

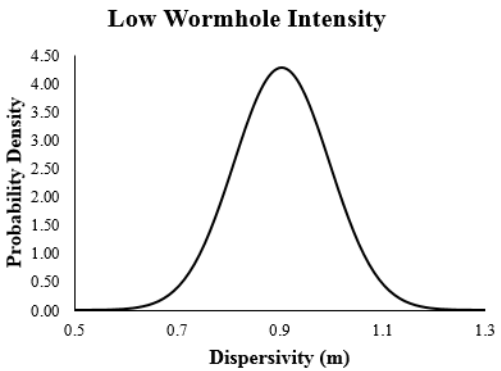

Mean	Variance
0.9039	0.0087

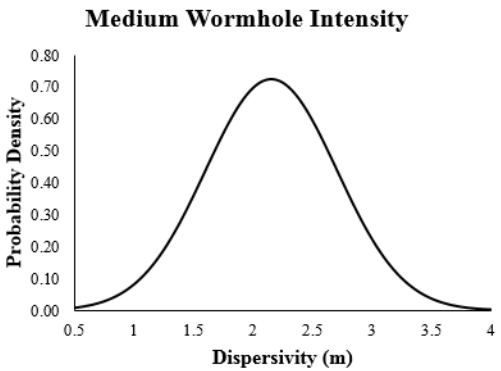

Mean	Variance
2.1571	0.3042

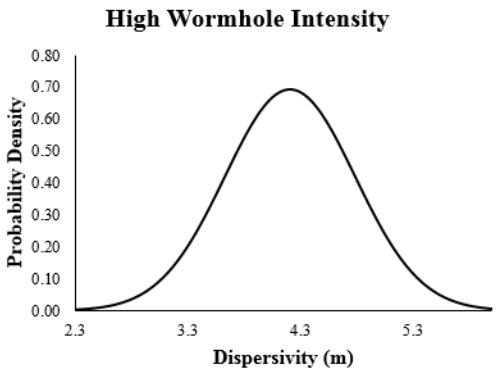

Mean	Variance
4.2111	0.3337

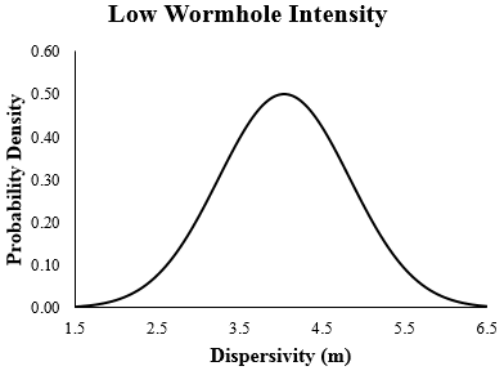

Mean	Variance
4.0429	0.6352

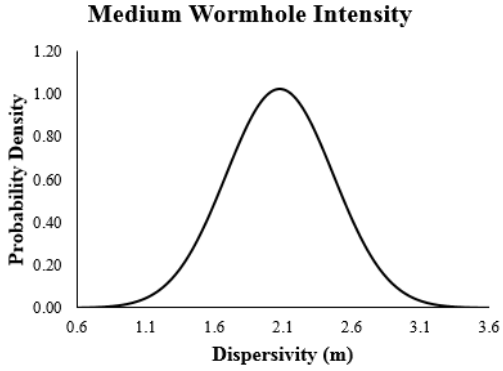

Mean	Variance
2.0793	0.1528

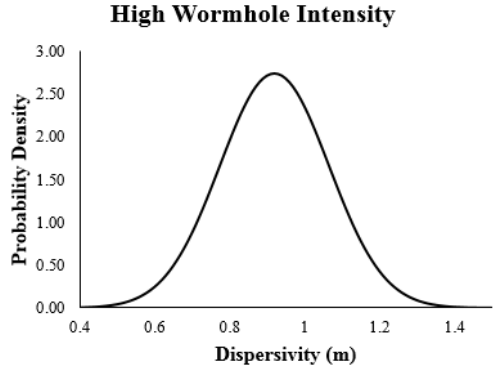

Mean	Variance
0.9207	0.0212

Fig. 3.15 – Fitted Gaussian distributions of dispersivity

Fracture System (top); Matrix System (bottom)

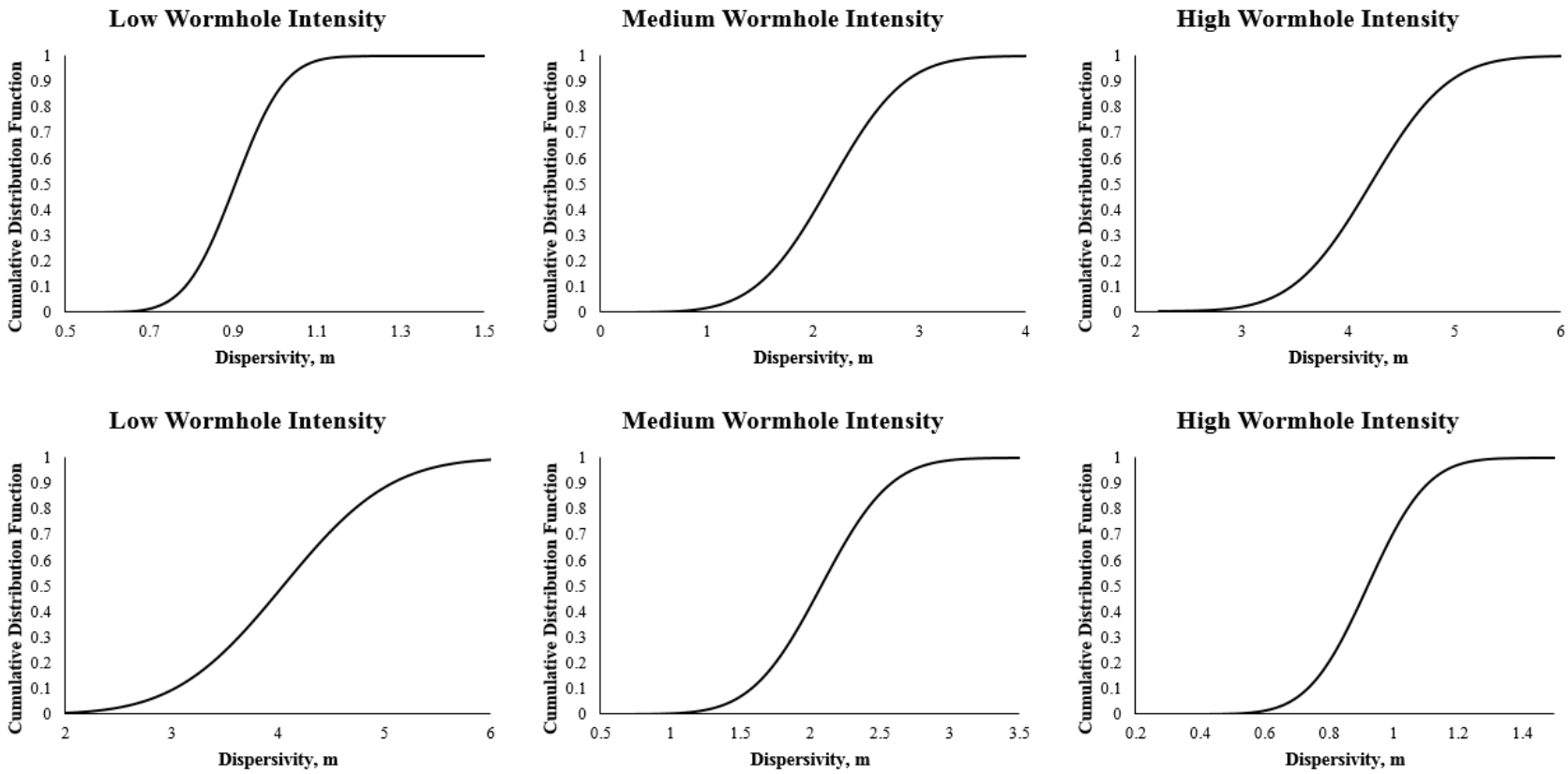

Fig. 3.16 – Cumulative distribution functions (CDFs)

Fracture System (top); Matrix System (bottom)

Chapter 4: Validation

4.1 Fine-Scale Model

Consider a field-scale model of 75-meter wide, 75-meter long, and 1-meter thick. For comparative purposes, models at two different resolutions are used. First, a high-resolution model is constructed, such that the complex wormhole pattern is explicitly represented in the computational domain. The model, as shown in Fig. 4.1, is 60 × 60 × 3 (Δx = 1.25 m; Δy = 1.25 m; Δz = 0.375, 0.25, and 0.375 m, respectively). The blocks containing the wormholes are locally refined (Δx = 0.25 m; Δy = 0.25 m; Δz = 0.25 m). The complex wormhole network extends in the middle layer. The initial conditions are the same as those presented in section 3.3. To mimic realistic field operating conditions, an injection period of 20 days, followed by 10 days of soaking, is modeled. The injection rate is modified from the calibration models in sections 3.3 and 3.4, in order to maintain the same injected pore volume.

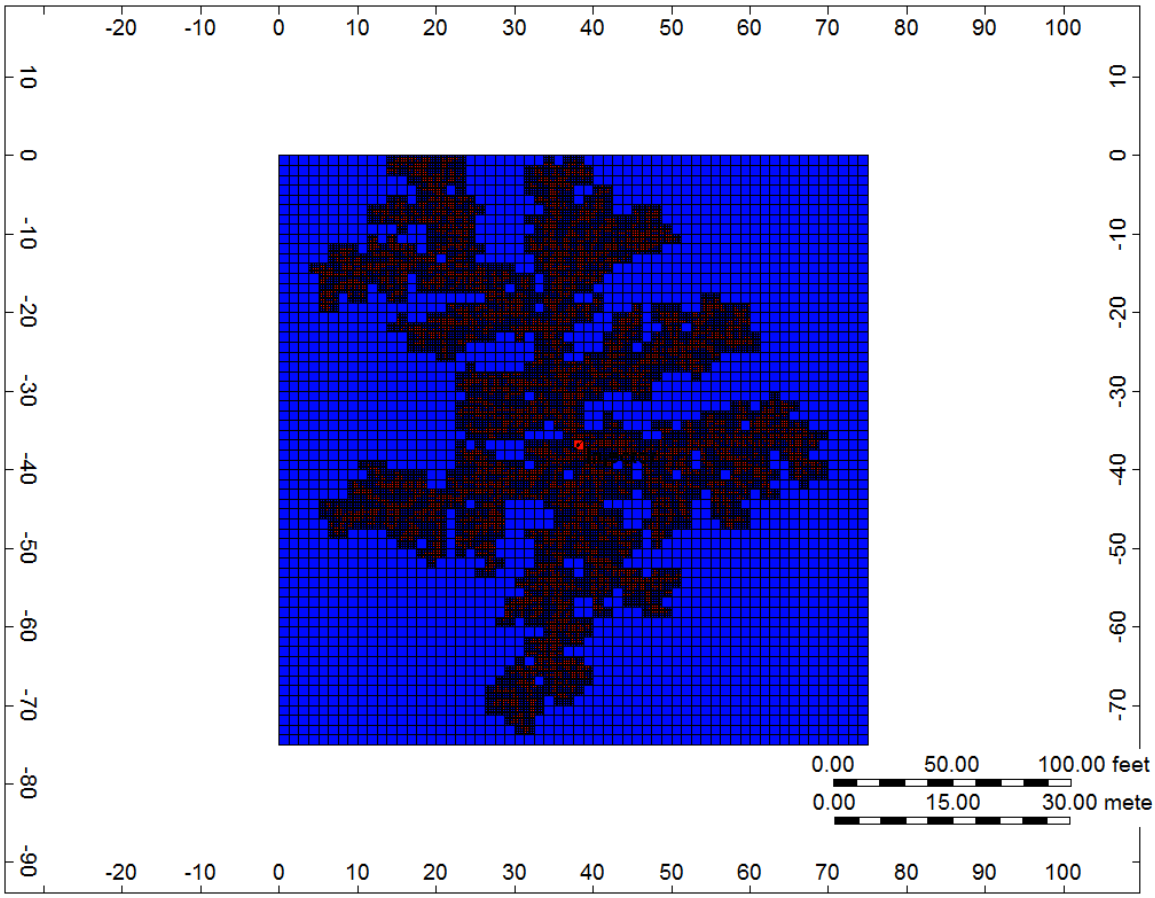

Fig. 4.1 – Fine-scale model

4.2 Coarse-Scale Model

Next, an equivalent dual-permeability continuum is constructed following the procedure described in section 3.4 as presented in Fig. 4.2. A total of 25 realizations of dispersivity values (fracture and matrix systems) are sampled, and their cumulative oil and gas production profiles are compared with the high-resolution model in Fig. 4.3.

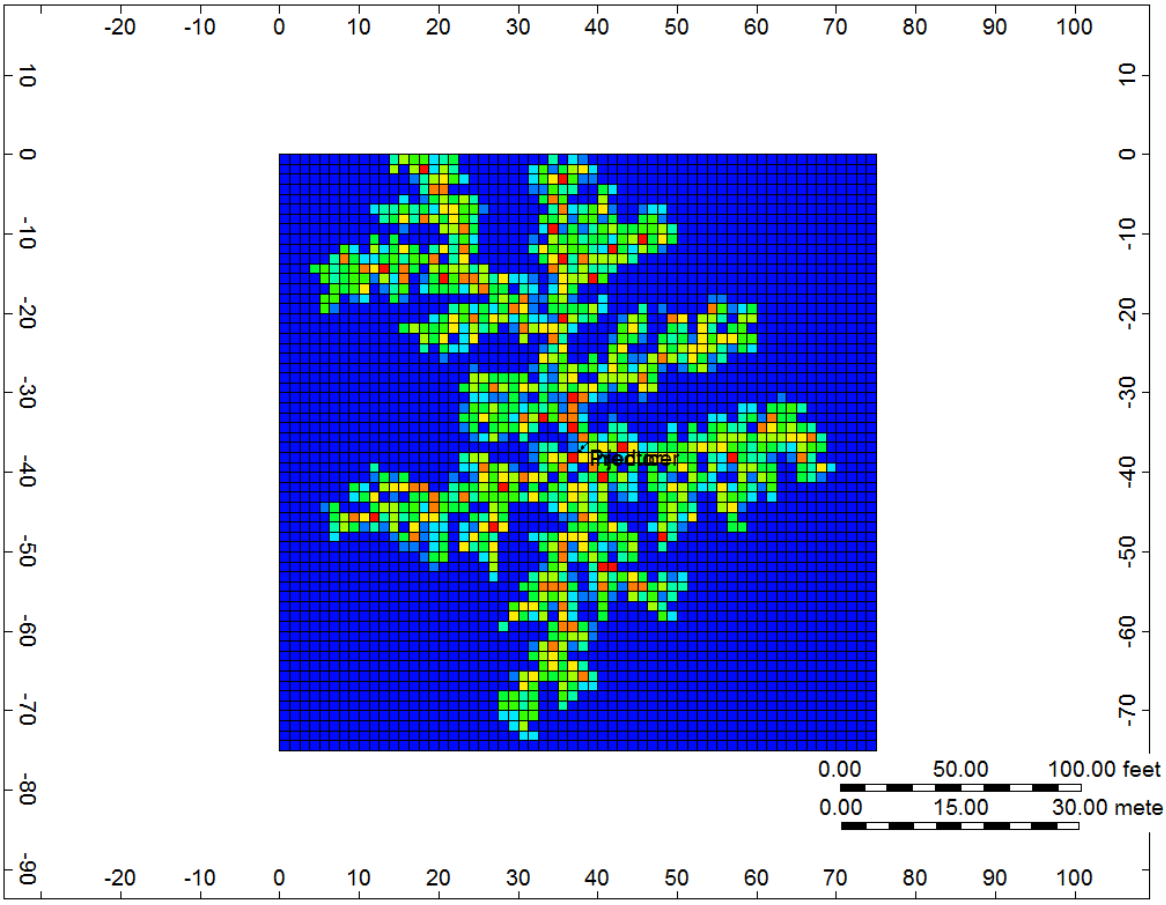

Fig. 4.2 – Coarse-scale model

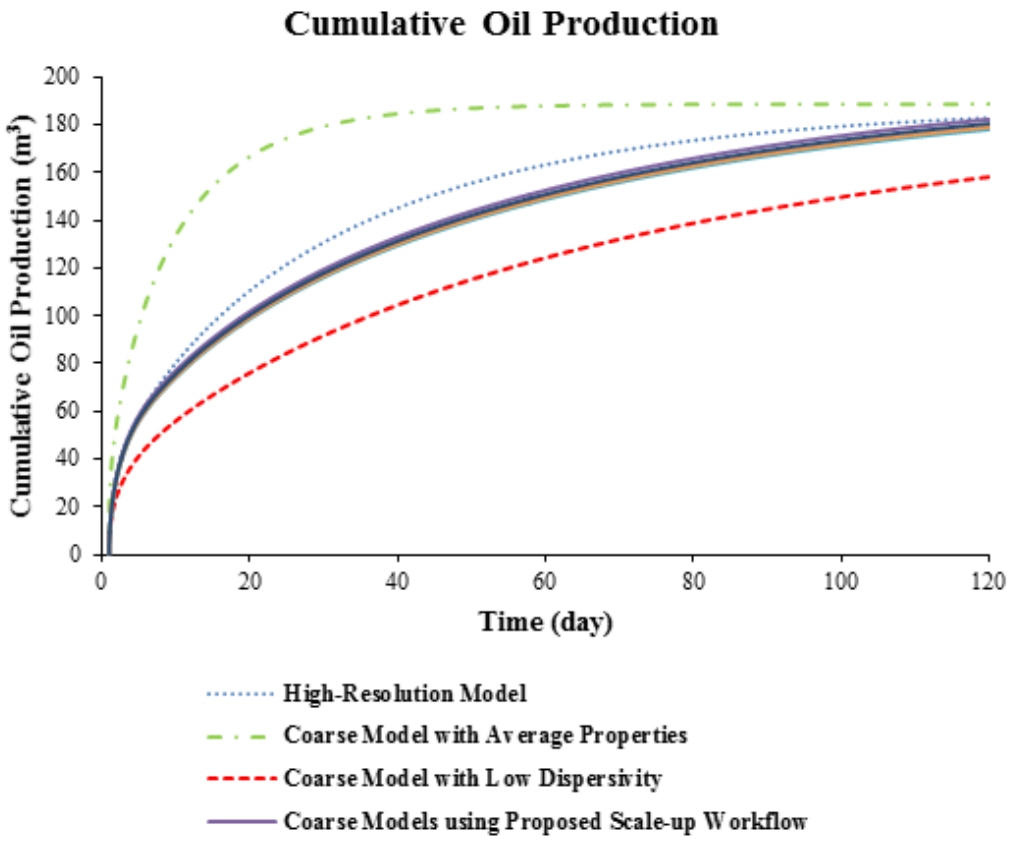

Fig. 4.3 – Cumulative oil production for the field-scale model

High-resolution model (blue); Coarse model with average properties (green); Coarse model with zero dispersivity (red); Coarse models following the proposed scale-up workflow (other colors)

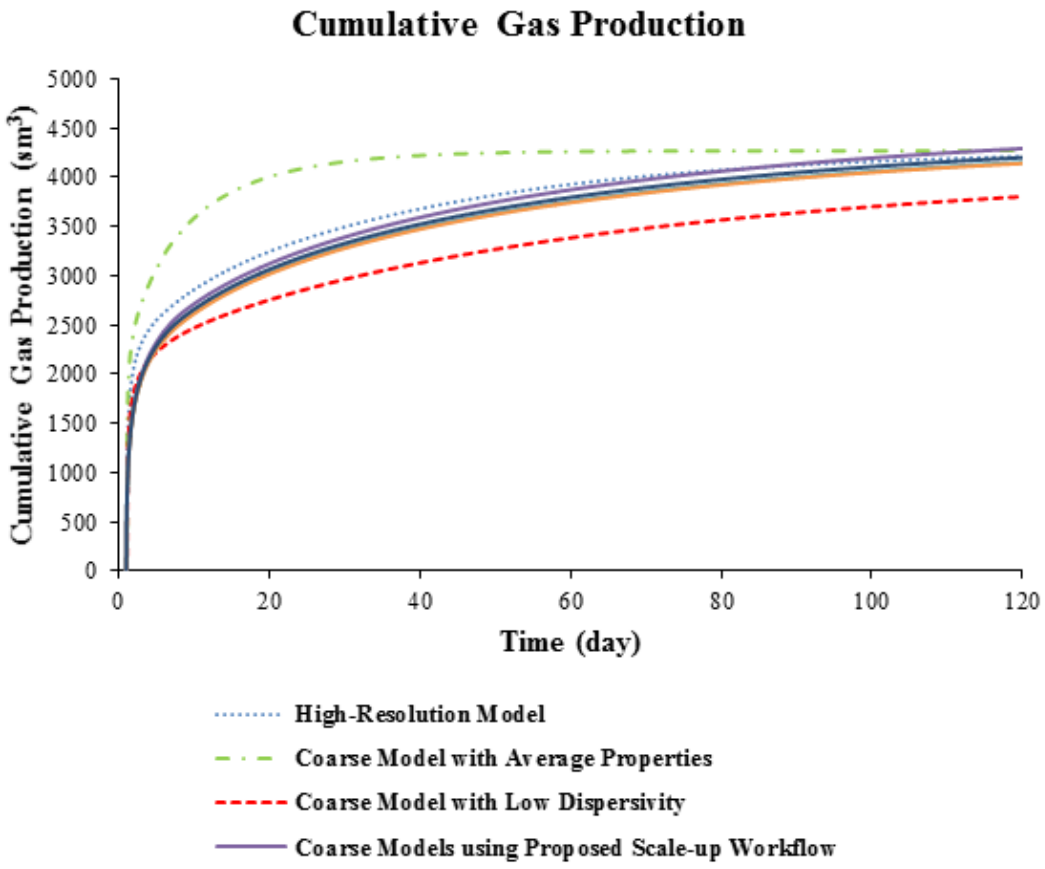

Fig. 4.4 – Cumulative gas production for the field-scale model

High-resolution model (blue); Coarse model with average properties (green); Coarse model with zero dispersivity (red); Coarse models following the proposed scale-up workflow (other colors)

Also shown in Fig. 4.3 and Fig. 4.4 are two additional cases of coarse models:

Green curve: constant WI of 45% (corresponding to a fracture spacing of 0.65 m) is assigned everywhere. This choice is based on an average WI value within a 12.5 m radius around the wellbore in the high-resolution model. The set-up depicts a scenario where the WI observed in the near wellbore region is mistakenly used to populate the entire model. Corresponding average dispersivity values of 4.21 m and 0.92 m are sampled from Fig. 3.13 for the fracture and matrix systems, respectively.

Red curve: constant WI of 72% (corresponding to a fracture spacing of 0.3 m) is assigned everywhere. Dispersivity is set to zero (same as the high-resolution model) everywhere.

Fig. 4.5 illustrates the solvent distribution at the end of the injection period for both the fine-scale and coarse-scale model, and Fig. 4.6 shows the oil saturation of the end of the production period.

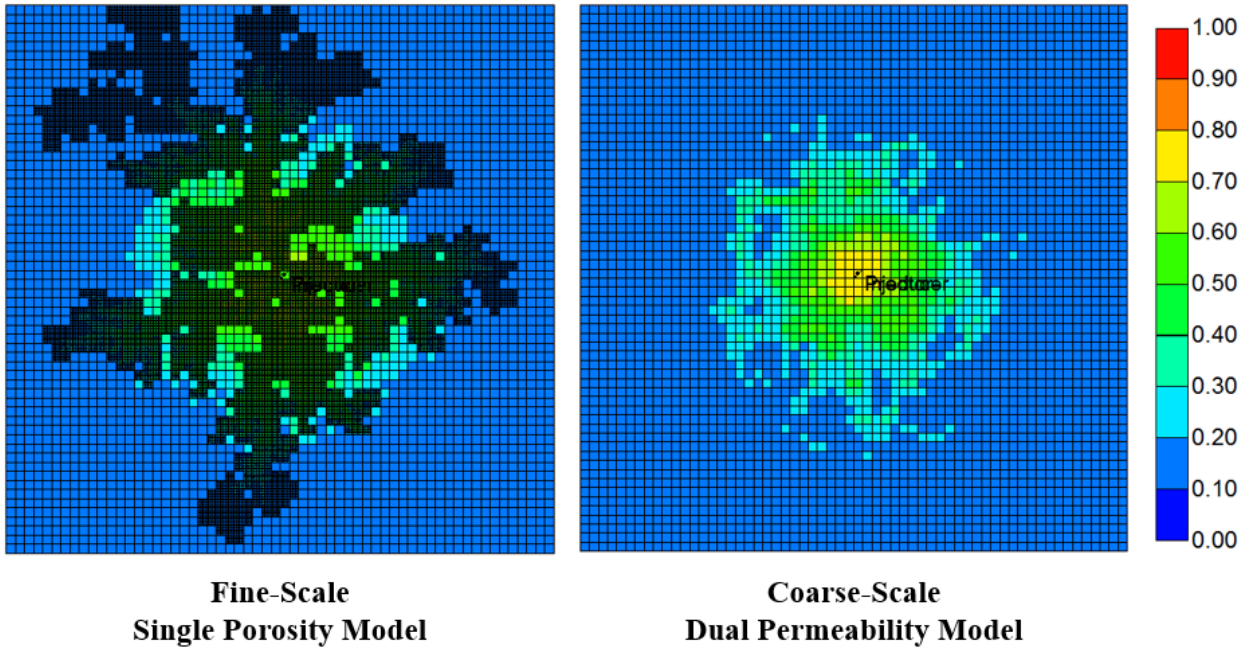

Fig. 4.5 – Solvent distribution at the end of injection period

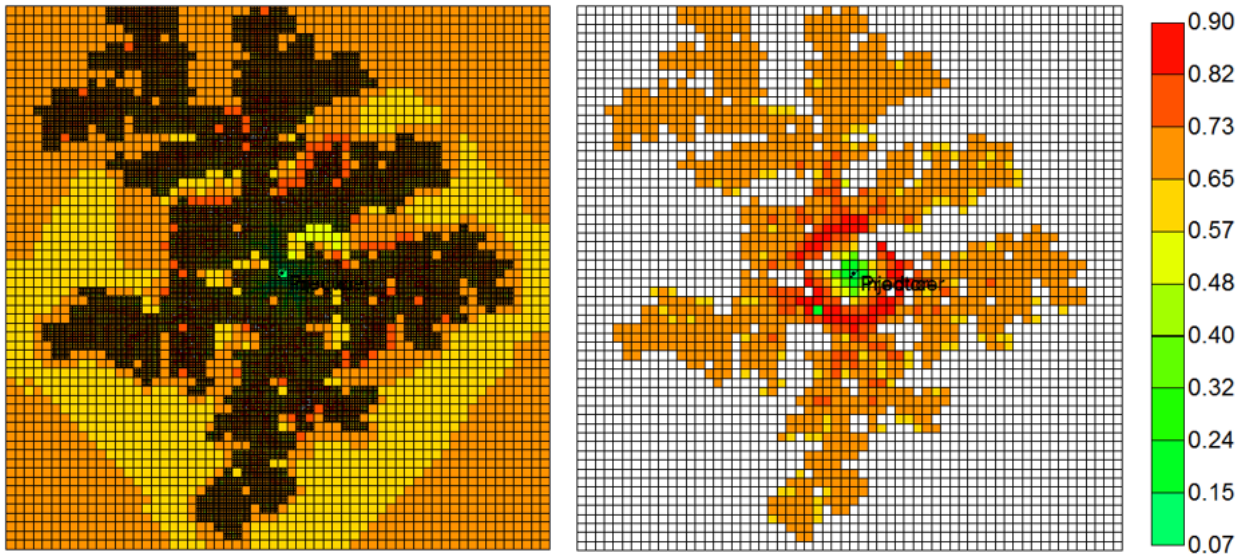

Fine-Scale
Single Porosity Model

Coarse-Scale
Dual Permeability Model

Fig. 4.6 – Oil saturation at the end of production period

4.3 Results and Discussion

The set-up described in the previous section (4.2) serves to illustrate the impact of not scaling up dispersivity and potentially underestimating solvent mixing in field-scale production. It is observed that results for the coarse models constructed according to the proposed workflow closely resemble those of the high-resolution model. Despite certain slight deviation at the early times, the profiles for the high-resolution model are completely encompassed by those of the coarse models during the late times. The importance of taking into account the sub-scale heterogeneities is clearly visible.

One of the main challenges in reservoir simulation is achieving a balance between accuracy and computational cost. This practical approach, involving a dual-permeability model, can offer the opportunity to reduce computational effort drastically as shown in Fig. 4.5. Reliable and efficient field-scale simulations with multiple well patterns can be performed by accounting for the contribution of sub-scale heterogeneities (wormhole configurations) in the transport and mixing of solvent and heavy oil in post-CHOPS applications.

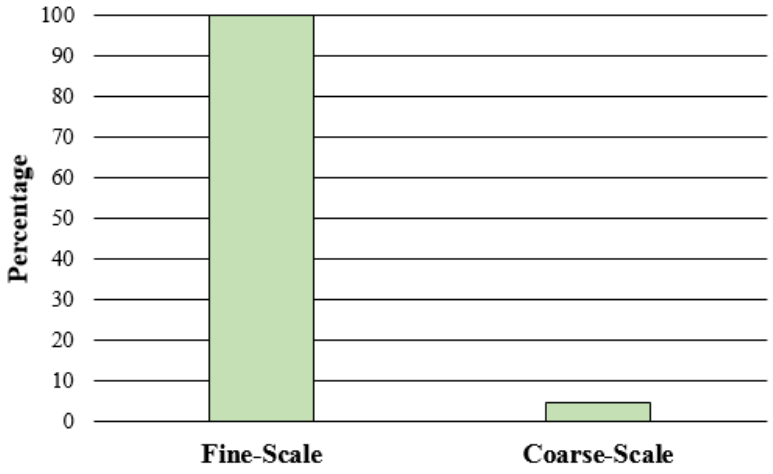

Fig. 4.7 – Reduction in computational time

Chapter 5: Design of Field-Scale Applications

This chapter focuses on the application of the proposed workflow to scale up solvent transport mechanisms in wormhole networks at a larger scale. The implementation of this workflow reduces the computational time significantly, which permits the proper assessment of multiple strategies to increase the recovery factor from post-CHOPS reservoirs by carrying out sensitivity analyses; several factors such as injection parameters, soaking time, and number of cycles are examined.

5.1 Injection Scheme

The main cost associated with most solvent-aided EOR applications is typically that of the solvent mixture. Provided that the solvent cost is highly dependent on the fluctuating market, the solvent volume available for injection could be identified as the key constraint for any potential application. A careful PVT study is always recommended in order to properly select the optimal solvent mixture for a particular heavy oil composition.

Once the solvent combination has been determined, the associated costs and its availability in field locations can be taken into account during the economic assessment of the project. The common approach in field operations is to keep injecting the selected solvent mixture until the reservoir pressure has returned to its initial value approximately (Chang and Ivory, 2013). Although this would be the ideal scenario, it is not always feasible due to the difficulty in maintaining an increasing trend in reservoir pressure, particularly when other nearby

wells are on production. Nevertheless, a proper injection scheme should aim to achieve partial miscibility between the solvent and heavy oil at the downhole pressures. For the field-scale model under consideration (75 m x 75 m x 3.5 m), the cumulative solvent injection profile is presented in Fig. 5.1. As discussed in section 3.2, the model is initially depleted to mimic the conditions and fluid distribution at the end of CHOPS. This pressure depletion process takes about six months with surface oil rates decreasing from 30 to 2 sm^3/day, where the final bottomhole pressure of 1,690 kPa is reached. A cut-off value of of 2 sm^3/day is set for the surface oil rate, as it is value commonly-adopted at most CHOPS wells (Dusseault, 2007).

In this case, the proposed injection scheme increases the average reservoir pressure from 1,690 kPa to its initial level (4,000 kPa), as illustrated in the pressure profile in Fig. 5.2. Once the desired reservoir pressure has been reached, solvent injection is stopped and the well is shut-in.

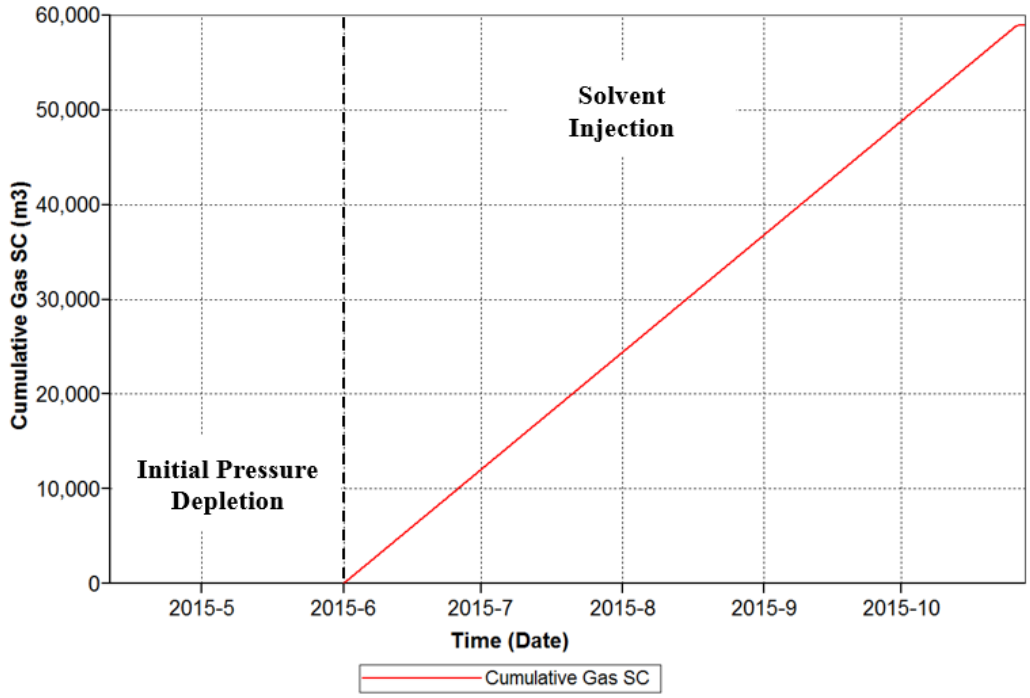

Fig. 5.1 – Cumulative solvent injection profile

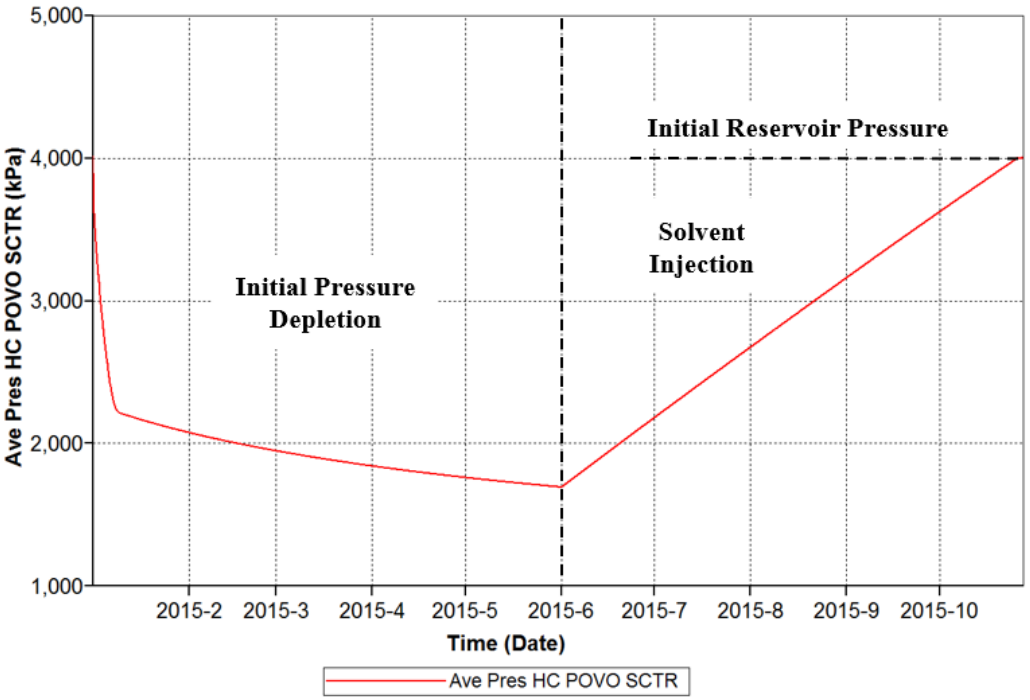

Fig. 5.2 – Average reservoir pressure profile

5.2 Optimal Soaking Time

As explained in previously, in most of the cases, the soaking duration is often arbitrarily selected or adopted from analog wells or previous applications. As a general rule of thumb, the soaking time should be at least half of the injection time, as evidenced in the pilot field applications (Husky Energy, 2011).

It would be reasonable to expect that longer soaking periods render a better recovery response. It is true that prolonged soaking times may increase the amount of heavy oil effectively contacted by the solvent, which would ultimately increase the final recovery factor. This postulation is supported by the following analysis, where different soaking times are examined, and the total recovery factors after a fixed production period of 190 days are presented in Table 5.1.

Table 5.1 – Recovery factor for different soaking times

Soaking Time (day)	Recovery Factor
10	9.24%
15	9.26%
18	9.26%
20	9.54%
22	9.54%
25	9.74%
30	10.01%

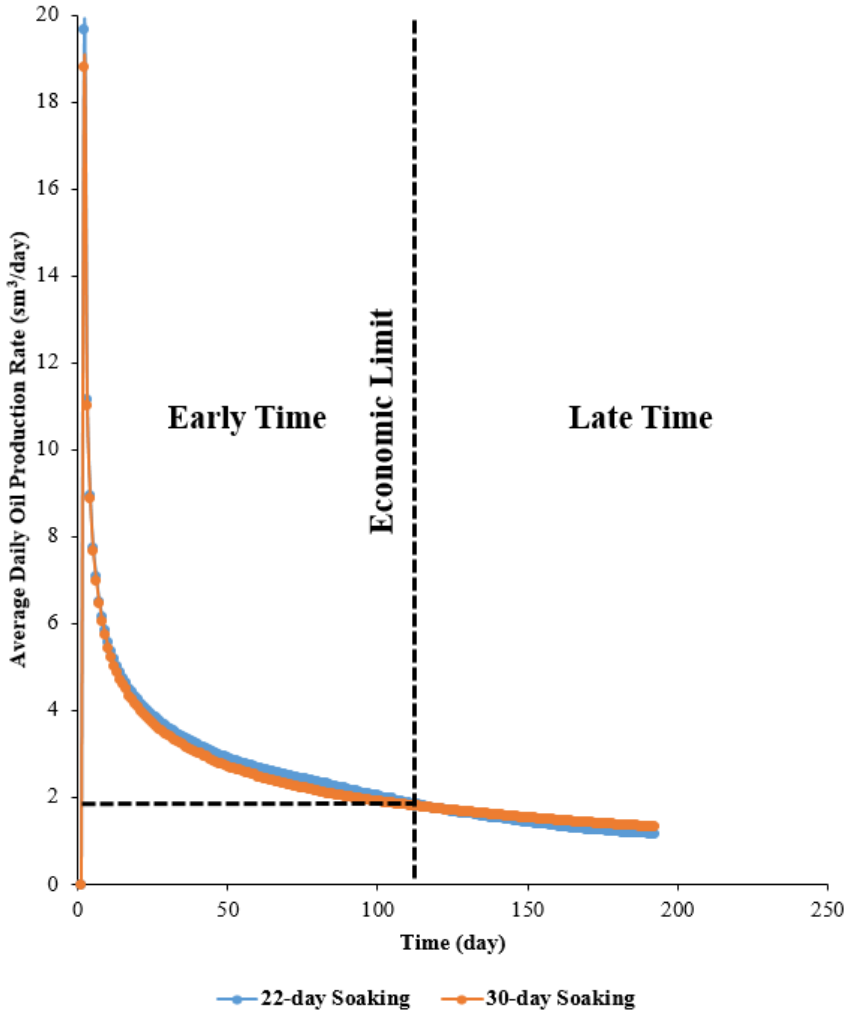

Fig. 5.3 – Oil surface rates for different soaking times

In addition, differences in decline profiles at early and late times corresponding to different soaking periods are also noted. For longer soaking periods, a slower decline at late times is identified; however, lower rate at early times is also observed. This difference is better illustrated by comparing the production profiles corresponding to two different soaking periods (22 days vs. 30 days) in Fig. 5.3. Comparing the saturation maps of these two cases (Fig. 5.4), the area that is effectively drained at the end of the production phase exhibit roughly the same

areal extent. By examining the corresponding solvent distribution in the wormhole networks in Fig. 5.5, it is evident that the solvent has effectively mobilized much of the oil from the drainage area after 22 days of soaking, reducing the oil viscosity and initiating additional solution-gas drive. However, as the soaking period continues to 30 days, the solvent has reached regions that are beyond the drainage area, diluting the solvent concentration in the near-well area, which contributes to the reduced initial oil production. Recovery of additional oil from regions that are far away would only contribute to the late-time production, when the rate has already declined considerably.

This difference of decline characteristics precisely explains why the 22-day case is the optimal one, if an economic limit of 2 sm^3/day, which represents the typical (post-) CHOPS constraint in Western Canada (Dusseault, 2007), is imposed. According to the results in Table 5.2, the optimal soaking time corresponding to the highest recovery factor up to the economic limit, is found to be 22 days. Comparing the 22-day and 30-day cases, it takes essentially the same number of producing days to reach the economic limit (115 days and 114 days for the 22-day and 30-day soaking periods, respectively).

The results support the conclusion that the economic limit would play an important role in determining the optimal soaking period. If the economic limit is zero, soaking the reservoir for extended periods of time would be ideal. In the end, the optimal condition depends on the trade-off between extracting additional oil recovery at late times versus producing at a higher rate at early times.

Table 5.2 – Recovery factor for different soaking times when an economic limit is enforced

Soaking Time (day)	Recovery Factor
10	6.83%
15	6.81%
18	6.45%
20	6.86%
22	7.21%
25	6.85%
30	6.85%

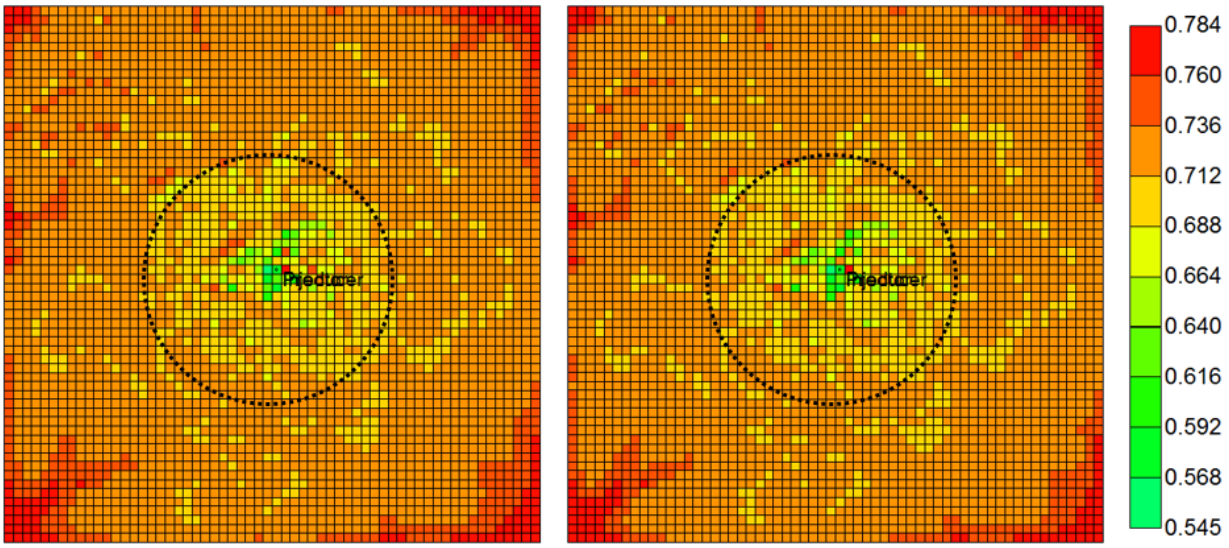

Fig. 5.4 – Oil saturation map after different soaking periods

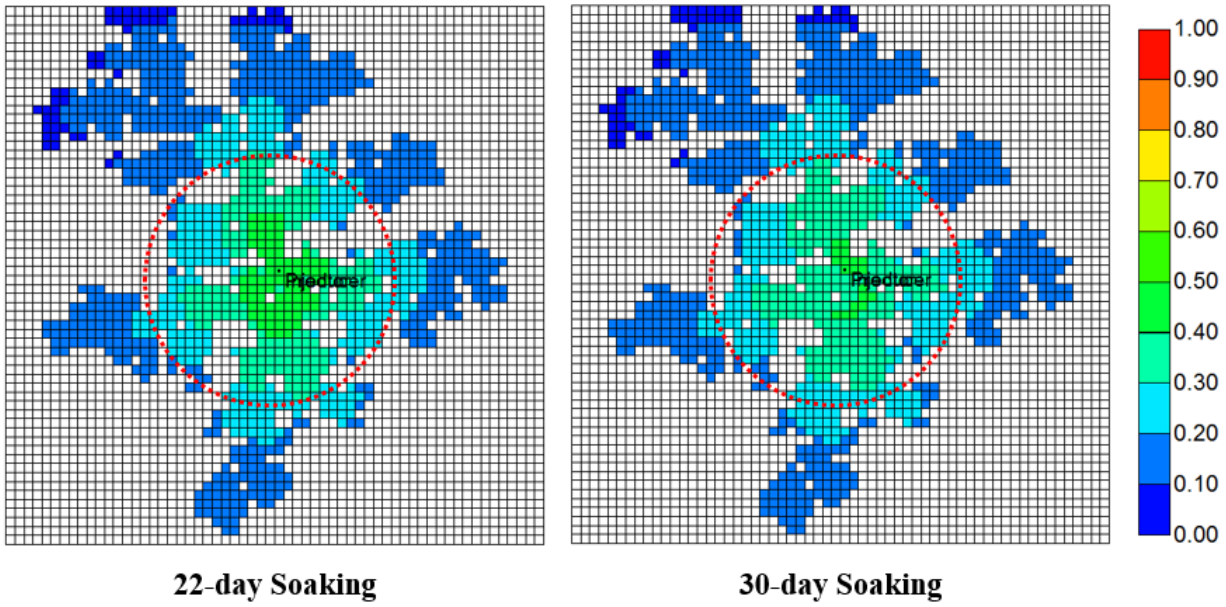

Fig. 5.5 – Global propane (solvent) distribution after different soaking periods

In the particular scenario that a lower oil production is not a constraint, soaking the reservoir for extended periods of time turns out to be more beneficial than shorter periods. Provided that time is not constraint, prolonged times increase the effective drainage area, which can be contacted by the solvent if long soaking periods are allowed, therefore mobilizing heavy oil from even further regions.

5.3 Number of Cycles

Given that previous studies typically model between two to six cycles in CSI operations, a total of six consecutive injection cycles are simulated. Each cycle consists of 30 days of injection at a rate of 300 sm^3/day, 20 days of soaking, and up to 100 days of production. Incremental recovery factors corresponding to each cycle are presented in Table 5.3 and illustrated in Fig. 5.6. Note that the first production cycle in Fig. 5.6 corresponds to the initial pressure depletion period (i.e., CHOPS), during which about 8.71% of the OOIP is recovered. The values in Table 5.3 are consistent with typical values reported in the literature (Ivory et al., 2010).

Table 5.3 – Incremental recovery factor after each cycle

Cycle / Stage	Additional Recovery Factor
Initial Pressure Depletion	8.71%
1st	6.88%
2nd	6.62%
3rd	6.21%
4th	5.66%
5th	4.59%
6th	2.96%

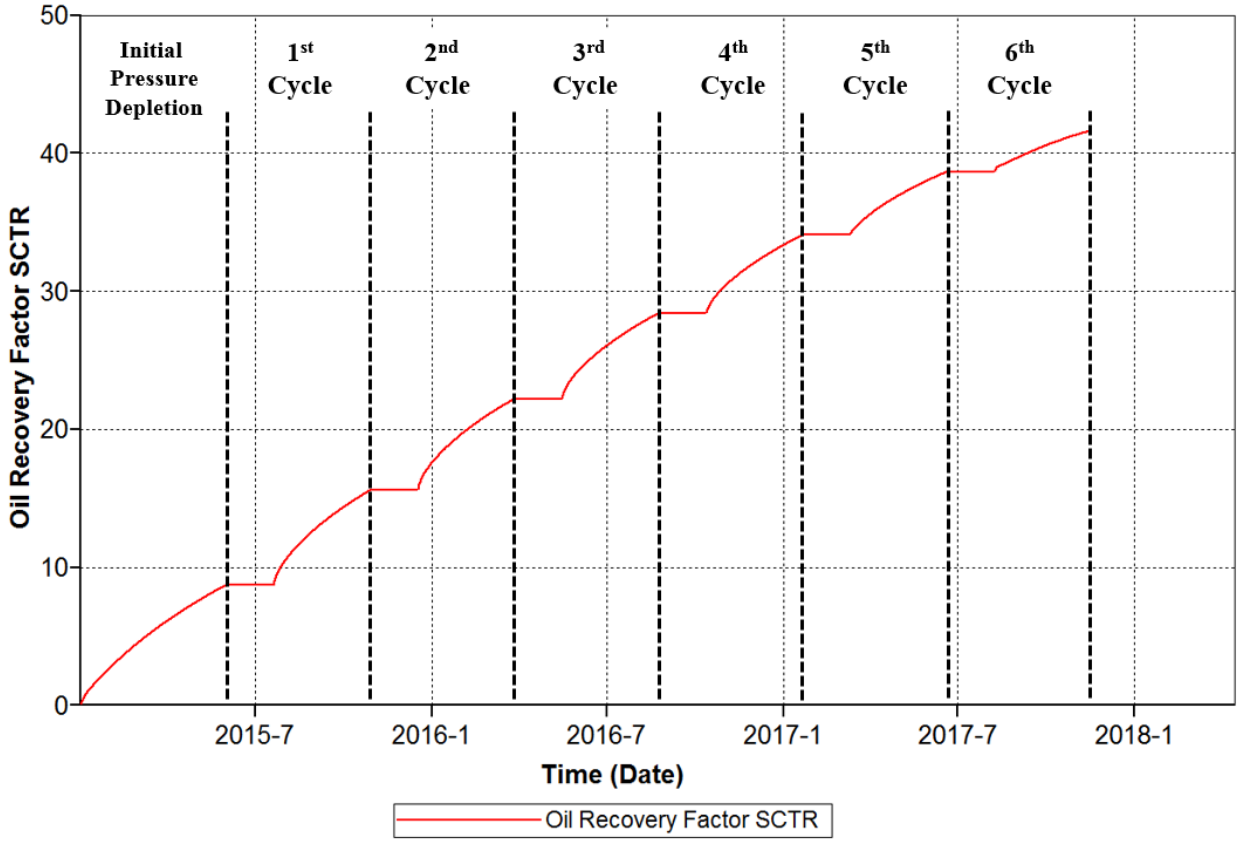

Fig. 5.6 – Cumulative recovery factor for six cycles

As expected, a decreasing trend in the incremental recovery factor with increasing cycle is observed (Fig. 5.7). The two initial cycles contribute most significantly to the overall oil recovery. If an economic rate in the range of 2 to 3 sm^3/day (16.8 to 25.2 bbl/day) is defined, the number of producing days would also exhibits a decreasing trend as evidenced in Fig. 5.8. Therefore, it is hypothesized that it would be more beneficial to implement fewer and longer cycles than more shorter cycles. This aspect will be explored further in the next section.

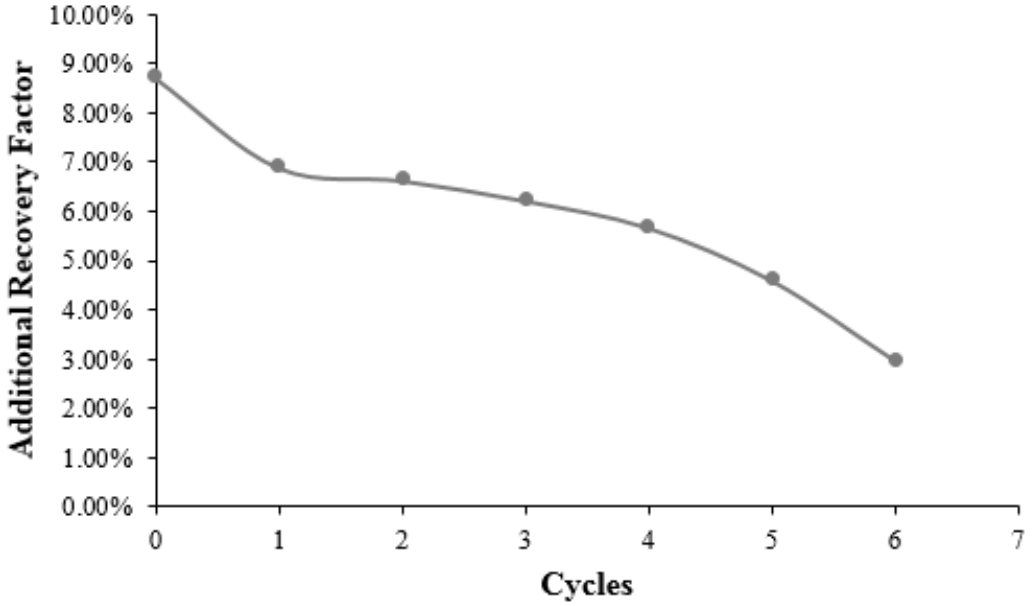

Fig. 5.7 – Incremental recovery factor after each cycle

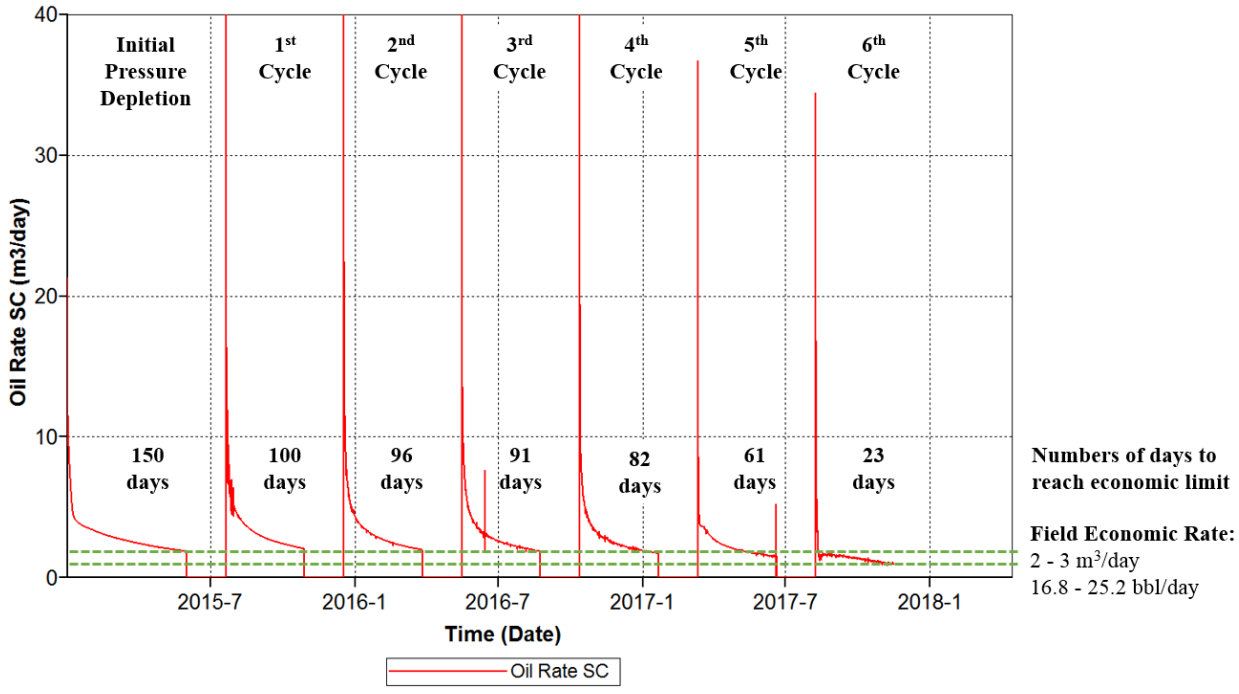

Fig. 5.8 – Surface oil rate in each cycle

Solvent efficiency can be assessed in terms of the solvent utilization factor (SUF), defined as the volume of oil recovered after injecting a unit volume of solvent (m^3 of oil produced per m^3 of solvent used). Inversely, the SUF can also be expressed as the amount of solvent required to produce a unit volume of incremental oil. The solvent utilization factor (SUF) for each one of the six cycles is presented in Table 5.4.

Table 5.4 – Solvent utilization factors (SUF) for each cycle

Cycle	SUF (sm^3 of Oil per sm^3 of Solvent)	SUF (sm^3 of Solvent per sm^3 of Oil)
1	0.0384	26.05
2	0.0370	27.05
3	0.0346	28.86
4	0.0316	31.63
5	0.0256	39.05
6	0.0166	60.42

5.4 Limited Amount of Solvent

As mentioned in section 5.1, the main cost associated with a CSI application is that of the solvent mixture. Therefore, a certain allocated budget would imply a fixed volume of solvent available for injection. In this section, a fixed solvent volume is imposed, and a multi-cycle approach is compared to a single consolidated cycle. In particular, two scenarios are examined: in the first case, the total volume of solvent is 18,000 m^3 and in the second case, a larger volume of 27,000 m^3 is employed.

5.4.1 Scenario 1

Two options are explored: in the first one, the entire amount of solvent (18,000 m^3) is injected in one single cycle, whereas in the second one, two equal amounts (9,000 m^3) are injected in two separate consecutive cycles. The objective is to examine any potential benefits, in terms of maximizing the ultimate recovery factor, with more cycles. To achieve a fair comparison, the total project lifespan is the same for both cases.

The results show that a slightly higher recovery factor is obtained from the single-cycle approach, as illustrated in Fig 5.9 and Table 5.5.

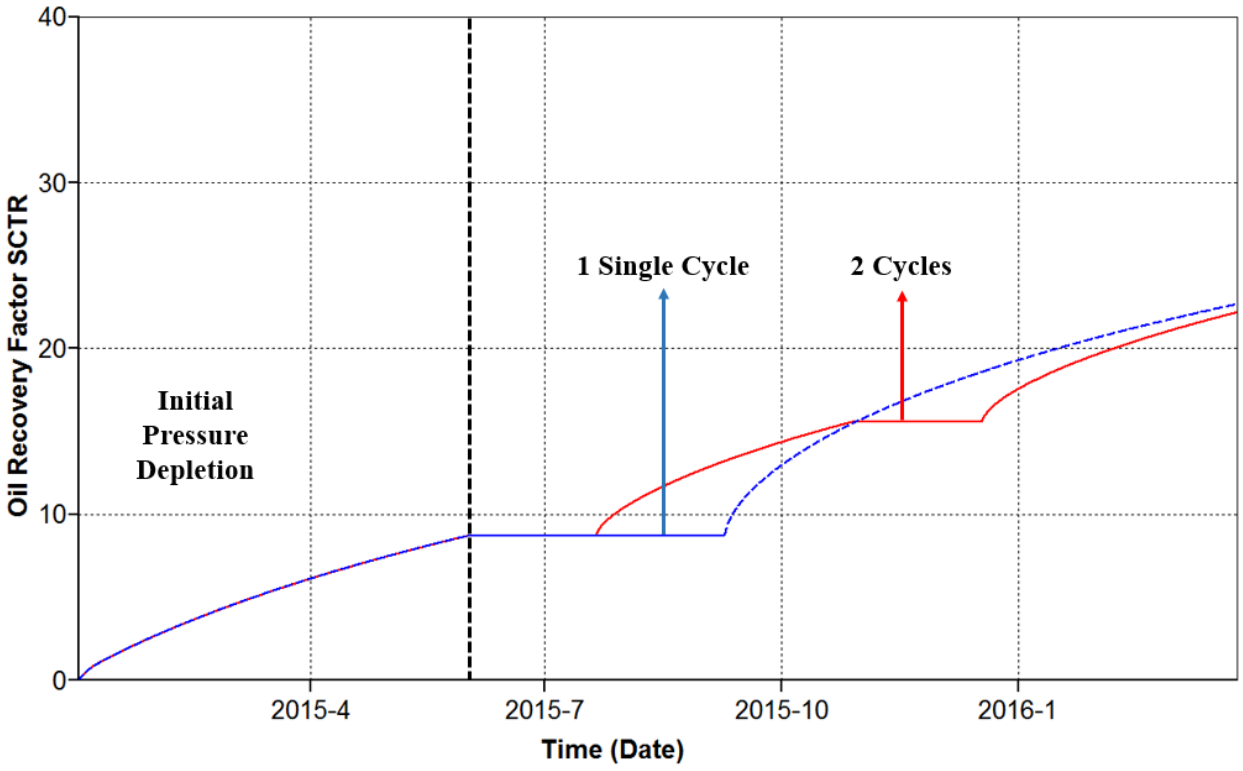

Fig. 5.9 – Oil recovery in one single cycle vs. two separate cycles

Table 5.5 – Recovery factor for Scenario 1

Type	Recovery Factor
2 Separate Cycles	1st: 15.58% 2nd: 7.11% Total: 22.19%
1 Combined Cycle	22.70%

5.4.2 Scenario 2

Once again, multi-cycle and single-cycle strategies are compared. Two options are explored: in the first one, the entire amount of solvent (27,000 m^3) is injected in one single cycle; in the second, three equal amounts (9,000 m^3) are injected in three separate consecutive cycles. Same observation as in 5.4.1 is noted: a slightly higher recovery factor is obtained from the first approach as illustrated in Fig. 5.10 and Table 5.6.

The results from these two scenarios appear to support the hypothesis that it would be more beneficial to implement fewer, longer cycles than multiple shorter cycles. Provided that the amount of solvent is fixed, it is then concluded that implementing one single cycle is likely to be more effective, in terms of recovery factor, than a series of shorter (injection-soaking-production) consecutive cycles.

Incorporating the findings from section 5.2, it is proposed that injecting larger volumes of solvent and extending the soaking times are recommended during the first and/or second cycles. In addition, when the amount of solvent available is limited, it would be more effective to inject

all the solvent in one single consolidated cycle, possibly with an extended soaking period, rather than performing shorter consecutive cycles.

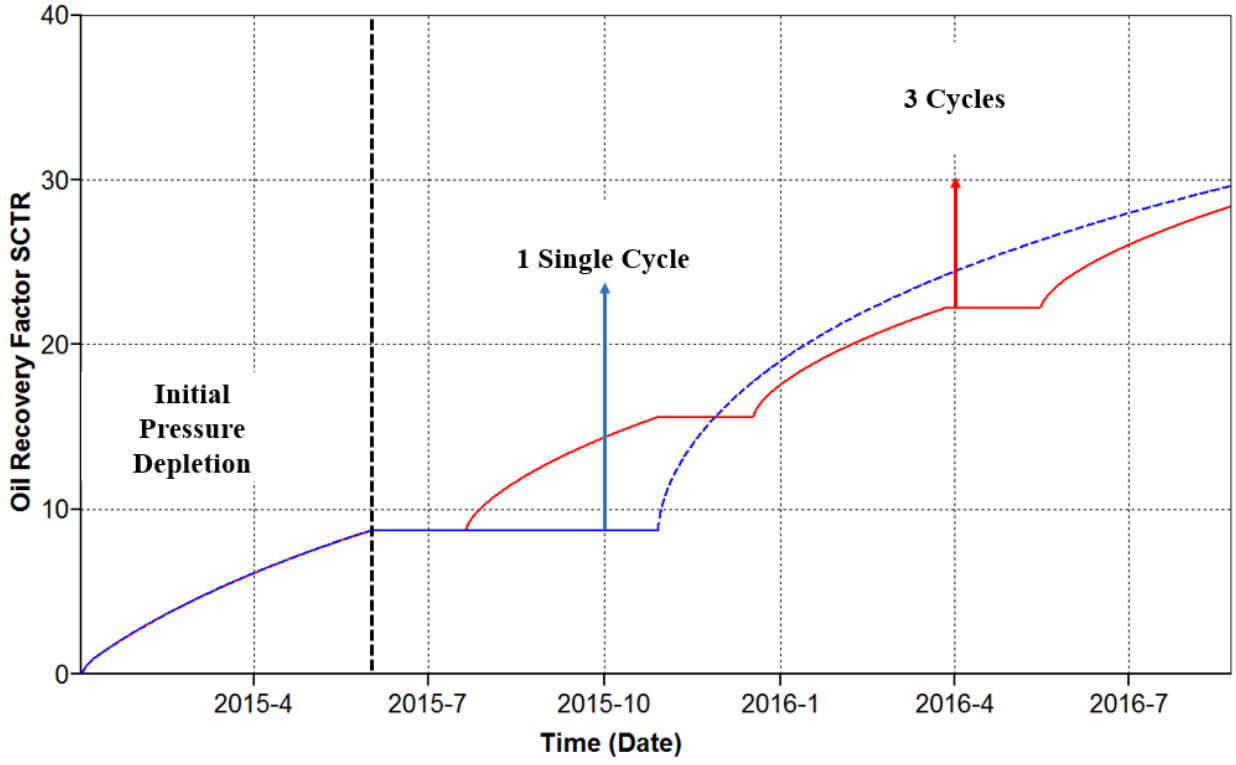

Fig. 5.10 – Oil recovery in one single cycle vs. three separate cycles

Table 5.6 – Recovery factor for Scenario 2

Type	Recovery Factor
3 Separate Cycles	1st: 15.58% 2nd: 7.11% 3rd: 5.68% Total: 28.37%
1 Combined Cycle	29.61%

Chapter 6: Conclusions and Recommendations for Future Work

6.1 Conclusions

This work presented a workflow to assign effective parameters in a dual-permeability continuum model for modeling post-CHOPS CSI processes. Variables including matrix/fracture porosity, fracture spacing, shape factors, and longitudinal/transverse dispersivities are computed in accordance with the fine-scale wormhole characteristics within a coarse-scale grid block. The calculation procedure is repeated over multiple realizations of wormhole configurations, allowing bivariate distributions of effective longitudinal/transverse dispersivities to be calibrated as functions of wormhole intensity. The calibrated distributions are used in a cloud transform procedure to construct models of effective dispersivities for field-scale simulations.

In contrast to many existing numerical analysis approaches that involve arbitrary adjustment of dispersivity via history matching, the developed workflow offers a novel and systematic framework to scale up solvent dispersivity in post-CHOPS applications. Fracture spacing, shape factor and dispersivity are assigned in a fashion that honors the realistic spatial variation in wormhole characteristics at the fine scale.

A synthetic case study involving typical petrophysical values and operational parameters for post-CHOPS reservoirs is presented. Shape factors and effective dispersivity values in the dual-permeability coarse models are assigned following the proposed workflow. In addition to > 90% reduction in computational time, results for the coarse models closely resemble those of the

high-resolution model. Except for some slight deviation during early times, the profiles for the high-resolution model are completely encompassed by those of the coarse models during the late times. The outcomes highlight the importance of properly capturing sub-scale heterogeneity effects during scale-up. The model is used to evaluate multiple production scenarios to assess the impacts of number and duration of CSI cycles on production efficiency.

Though previous numerical studies have examined the optimization of CSI processes, a lack of proper scale-up procedures has rendered their description of heterogeneous wormhole networks at the field scale incomplete, which could potentially compromise the reliability of the corresponding optimization results. It is argued that the model employed in this study could better represent the detailed wormhole features at the coarse scale; hence, it is more appropriate for field-scale operations design. The aforementioned scale-up procedure was implemented to construct coarse-scale simulation models to provide insights on operational strategies and key considerations when optimizing cyclic solvent injection (CSI) processes in field-scale applications:

- Extended soaking period could positively impact the ultimate oil recovery, but it also inadvertently lowers the early production. The optimal soaking period is a function of the economic limit, as it reflects a trade-off between extracting additional oil recovery at late times versus producing at a higher rate at early times.
- The results support the hypothesis that it is more effective to implement fewer, but longer, cycles instead of more, yet shorter, cycles. In particular, if the amount of solvent is limited, it would be more effective to inject all the solvent in one single consolidated cycle, possibly with an extended soaking period, rather than performing shorter

consecutive cycles. Generally speaking, it is recommended to inject larger volumes of solvent and extending the soaking times during the first and/or second cycles.

6.2 Future Work

This systematic workflow can be extended to incorporate other foamy-oil modeling approaches, such as the kinetic and the pseudo-bubble point models, to assess the impact of pressure depletion strategies on the non-equilibrium foamy oil behavior.

Future studies should focus on the application of this practical workflow to model multiple production scenarios to assess the impacts of pressure depletion schedule in the solvent transport and to study the interactions between wormhole characteristics and non-equilibrium phase behavior (e.g., solution or dissolution of foamy oil; distribution of free gas during post-CHOPS) at the field-scale using kinetic approaches.

Bibliography

Babadagli, T., & Rangriz-Shokri, A. (2013, June). Modeling Thermal and Solvent Injection Techniques as Post-CHOPS Applications Considering Geomechanical and Compositional Effects. Presented at the *SPE Heavy Oil Conference-Canada* held in Calgary, Canada June 11-13. Society of Petroleum Engineers.

Bera, A., & Babadagli, T. (2016). Relative permeability of foamy oil for different types of dissolved gases. *SPE Reservoir Evaluation & Engineering*, *19*(04), 604-619.

Chang, J., & Ivory, J. (2013). Field-scale simulation of cyclic solvent injection (CSI). *Journal of Canadian Petroleum Technology*, *52*(04), 251-265.

Chang, J., & Ivory, J. (2015, June). History Match and Strategy Evaluation for CSI Pilot. Presented at the *SPE Canada Heavy Oil Technical Conference* held in Calgary, Canada June 9-11. Society of Petroleum Engineers.

Chang, J., Ivory, J., & London, M. (2015, June). History Matches and Interpretation of CHOPS Performance for CSI Field Pilot. Presented at the *SPE Canada Heavy Oil Technical Conference* held in Calgary, Canada June 9-11. Society of Petroleum Engineers.

Claridge, E. L. (1994). A Proposed Model and Mechanism for Anomalous Foamy Heavy Oil Behavior. Presented at the *International Heavy Oil Symposium* held in Calgary, Canada June 19-21. Society of Petroleum Engineers.

Computer Modelling Group Ltd. (2016). GEM Compositional & Unconventional Reservoir Simulator - User Guide.

Computer Modelling Group Ltd. (2016). WinProp Phase-Behaviour & Fluid Property Program - User Guide.

Denney, D. (1999). Wormhole-Network Model of Cold Production in Heavy Oil. *Journal of Petroleum Technology*, *51*(09), 102-104.

Du, Z., Zeng, F., & Chan, C. (2015). An experimental study of the post-CHOPS cyclic solvent injection process. *Journal of Energy Resources Technology*, *137*(4), 042901.

Fan, Z., & Yang, D. (2016, April). Characterization of Wormhole Growth and Its Applications for CHOPS Wells Using History Matching. Presented at the *SPE Improved Oil Recovery Conference* held in Tulsa, USA April 11-13. Society of Petroleum Engineers.

Fan, Z., & Yang, D. (2017, February). Quantification of Sand Production by Use of a Pressure-Gradient-Based Sand Failure Criterion. Presented at the *SPE Canada Heavy Oil Technical Conference* held in Calgary, Canada February 15-16. Society of Petroleum Engineers.

Fan, Z., Yang, D., & Li, X. (2017, May). Determination of Three-Phase Relative Permeability in CHOPS Processes by Use of an Improved Iterative Ensemble Smoother. Presented at the *SPE Reservoir Characterization and Simulation Conference and Exhibition* held in Abu Dhabi, UAE. Society of Petroleum Engineers.

Firoozabadi, A. (2001). Mechanisms of solution gas drive in heavy oil reservoirs. *Journal of Canadian Petroleum Technology*, *40*(03), 15-20.

Haddad, A. S., & Gates, I. (2015). Modelling of Cold Heavy Oil Production with Sand (CHOPS) using a fluidized sand algorithm. *Fuel*, *158*, 937-947.

Husky Energy. (2011, November 30). Husky Oil's Mervin Cold Solvent EOR Pilot Final Technical Report for the SPRO Program. Saskatchewan Petroleum Research Incentive.

Istchenko, C. M., & Gates, I. D. (2014). Well/Wormhole model of cold heavy-oil production with sand. *SPE Journal*, *19*(02), 260-269.

Istchenko, C., & Gates, I. D. (2011, January). The well-wormhole model of cold production of heavy oil reservoirs. Presented at the *SPE Heavy Oil Conference and Exhibition* held in Kuwait City, Kuwait. Society of Petroleum Engineers.

Ivory, J., Chang, J., Coates, R., & Forshner, K. (2010). Investigation of cyclic solvent injection process for heavy oil recovery. *Journal of Canadian Petroleum Technology*, *49*(09), 22-33.

Jia, X., Li, J., Chen, Z., Gu, Y., & Zeng, F. (2016, May). Modeling of Foamy-Oil Flow in Solvent-Based Recovery Processes. Presented at the *SPE EUROPEC featured at 78th EAGE Conference and Exhibition* held in Vienna, Austria. Society of Petroleum Engineers.

Kraus, W. P., McCaffrey, W. J., & Boyd, G. W. (1993, January). Pseudo-bubble point model for foamy oils. Presented at the *Annual Technical Meeting* held in Calgary, Canada. Petroleum Society of Canada.

Lebel, J. P. (1994, March). Performance implications of various reservoir access geometries. In *11th Annual Heavy Oil & Oil Sands Tech. Symp., March* (Vol. 2).

Li, H., Zheng, S., & Yang, D. T. (2013). Enhanced swelling effect and viscosity reduction of solvent (s)/CO2/heavy-oil systems. *SPE Journal*, *18*(04), 695-707.

Li, X., Yin, Y., Yang, Z., Shen, Y., & Liu, Z. (2016, June). Produced Gas Reinjection Based Cyclic Solvent Processes for Foamy Oil Reservoirs in the Eastern Orinoco Belt, Venezuela. Presented at the *SPE Canada Heavy Oil Technical Conference* held in Calgary, Canada June 7-9. Society of Petroleum Engineers.

Liu, X., & Zhao, G. (2005). A fractal wormhole model for cold heavy oil production. *Journal of Canadian Petroleum Technology*, *44*(09).

Maini, B. B. (2001). Foamy-oil flow. *Journal of Petroleum Technology*, *53*(10), 54-64.

Martinez-Gamboa, J. J., Wang, M., & Leung, J. Y. (2017, May). A Practical Approach for Scale-Up of Solvent Transport Mechanisms in Post-CHOPS EOR Applications. Presented at the *SPE Latin America and Caribbean Petroleum Engineering Conference* held in Buenos Aires, Argentina May 17-19. Society of Petroleum Engineers.

Naderi, K., & Babadagli, T. (2016). Solvent Selection Criteria and Optimal Application Conditions for Heavy-Oil/Bitumen Recovery at Elevated Temperatures: A Review and Comparative Analysis. *Journal of Energy Resources Technology*, *138*(1), 012904.

Naderi, K., Romaniuk, N., & Ozum, B. (2015, October). Improvement of the CHOPS Process Efficiency. Presented at the *SPE Kuwait Oil and Gas Show and Conference* held in Mishref, Kuwait October 11-14. Society of Petroleum Engineers.

Pooladi-Darvish, M., & Firoozabadi, A. (1999). Solution-gas drive in heavy oil reservoirs. *Journal of Canadian Petroleum Technology*, *38*(04).

Rangriz-Shokri, A., & Babadagli, T. (2015). Field-Scale Deformation Analysis of Cyclic Solvent Stimulation in Thin Unconsolidated Heavy-Oil Reservoirs with Developed Wormhole Network. *Journal of Canadian Petroleum Technology*, *54*(06), 341-350.

Rangriz-Shokri, A., & Babadagli, T. (2016). A Sensitivity Analysis of Cyclic Solvent Stimulation for Post-CHOPS EOR: Application on an Actual Field Case. *SPE Economics & Management 8*(04), 78-89.

Rangriz-Shokri, A. R., & Babadagli, T. (2014). Modelling of Cold Heavy-Oil Production with Sand for Subsequent Thermal/Solvent Injection Applications. *Journal of Canadian Petroleum Technology*, *53*(2), 95-108.

Rangriz-Shokri, & Babadagli, T. (2016). Field scale modeling of CHOPS and solvent/thermal based post CHOPS EOR applications considering non-equilibrium foamy oil behavior and realistic representation of wormholes. *Journal of Petroleum Science and Engineering*, *137*, 144-156.

Sheng, J. J., Maini, B. B., Hayes, R. E., & Tortike, W. S. (1999). Critical review of foamy oil flow. *Transport in Porous Media*, *35*(2), 157-187.

Soh, Y. J., Rangriz-Shokri, A., & Babadagli, T. (2016, September). A New Modeling Approach to Optimize Methane-Propane Injection in a Field after CHOPS. Presented at the *SPE Annual Technical Conference and Exhibition* held in Dubai September 26-28. UAE. Society of Petroleum Engineers.

Speight, J. G. (2013). *Enhanced recovery methods for heavy oil and tar sands*. Elsevier.

Sun, X., Dong, M., Zhang, Y., & Maini, B. B. (2015). Enhanced heavy oil recovery in thin reservoirs using foamy oil-assisted methane huff-n-puff method. *Fuel*, *159*, 962-973.

Tremblay, B., Sedgwick, G., & Forshner, K. (1996, January). Modelling of sand production from wells on primary recovery. Presented at the *Annual Technical Meeting* held in Calgary, Canada. Petroleum Society of Canada.

Tremblay, B., Sedgwick, G., & Forshner, K. (1997). Simulation of cold production in heavy-oil reservoirs: wormhole dynamics. *SPE Reservoir Engineering*, *12*(02), 110-117.

Vishal, V., & Leung, J. Y. (2015). Modeling impacts of subscale heterogeneities on dispersive solute transport in subsurface systems. *Journal of contaminant hydrology*, *182*, 63-77.

Yang, P., Li, H., & Yang, D. (2014). Determination of Saturation Pressures and Swelling Factors of Solvent (s)–Heavy Oil Systems under Reservoir Conditions. *Industrial & Engineering Chemistry Research*, *53*(5), 1965-1972.

Yuan, J. Y., Tremblay, B., & Babchin, A. (1999). A wormhole network model of cold production in heavy oil. Presented at the *SPE International Thermal Operations and Heavy Oil Symposium* held in Bakersfield, USA March 17-19. Society of Petroleum Engineers.

Zhang, M., Du, Z., Zeng, F., Hong, S. Y., & Xu, S. (2016). Upscaling study of the cyclic solvent injection process for post-CHOPS reservoirs through numerical simulation. *The Canadian Journal of Chemical Engineering*, *94*(7), 1402-1412.